UNIVERSITA' DEGLI STUDI DI PADOVA

DIPARTIMENTO DI SCIENZE CHIMICHE

CORSO DI LAUREA MAGISTRALE IN CHIMICA

TESI DI LAUREA MAGISTRALE

ELECTROCHEMICAL STUDY ON THE CATALYTIC ACTIVITY OF Fe-N-C MATERIALS IN THE ACTIVATION AND FIXATION OF CO_2 IN ACETONITRILE

Relatore: Prof. Durante Christian

Controrelatore: Prof. Zonta Cristiano

LAUREANDO: Cesca Davide

ANNO ACCADEMICO 2021/2022

to those who are lost

to what I have lost

In memoria di E.C.

Abstract

The electrochemical reduction of carbon dioxide is a promising way to transform this gas into a useful resource. The Fe-N-doped carbons are emerging noble metal free electrocatalysts where the active site is represented by an iron metal centre coordinating 4 nitrogen atoms, in a structure similar to that observed in porphyrin or phthalocyanine molecular systems. However, while the study and use of Fe-N-C catalysts is widely documented in aqueous electrolytes even for the CO_2 reduction reaction, their behaviour in organic solvent is poorly investigated. This is somehow astonishing since metal porphyrin/phtalocyanine molecular systems have been used and characterized since the sixties of the last century to catalyse, in homogeneous phase, the reactivity of small molecules including CO_2 itself. This thesis work tries to fit into this context trying to fill this gap. In this thesis, Fe-N-C catalysts were tested in acetonitrile, a solvent with ca. 10 times higher CO_2 solubility than water. Three types of Fe-N-doped catalysts, differing for the % of FeN_4 sites, were tested for the direct reduction of CO_2 and the fixation of CO_2 using organic halides. It was found that the direct reduction of CO_2 is not catalysed on F-N-doped carbons, but the cleavage of the C-Cl bond was catalysed and anticipated of 300 mV with respect to the glassy carbon electrode. However, even in this case the catalytic action seems to be due not to the presence of FeN_4 sites but to the presence of nitrogen functional groups such as pyridine, pyrrole or N-graphite. This has allowed to hypothesize the use of Fe-N-C systems for dehalogenation reaction as well as for the *in-situ* formation of nucleophilic species available to react for example with CO_2 to give carboxylation reaction. In particular, the dehalogenation reaction of benzyl chloride has been studied. The reaction occurs through a concerted mechanism, where the first electron transfer leads directly to the breaking of the carbon-halogen bond with the formation of a radical which is rapidly reduced to a carbanion. In the presence of CO_2 the carbanion leads to the formation of phenylacetic acid, which however, given the applied potential, undergoes further reduction reaction to the corresponding carbonate.

Summary

1 Introduction

1.1 CO_2 utilization

The increasing levels of greenhouse gases caused by human activities are reaching a tipping point. Particularly upsetting is the high level of CO_2 in the atmosphere, the highest value ever recorded. Since the Kyoto protocol the world most industrialized countries are trying to restrain the future damages caused by the raising of the average global temperature, encouraging green solutions, and funding innovative research to the problems.

One of the main roads toward a sustainable future is storing and recycling CO_2 to lower its level in the atmosphere and achieve a "net-zero carbon" economy. Storage methods for CO_2 are already available but not exploited on large scale plants, despite the special report of the Intergovernmental Panel on Climate Change (IPCC) [1] saying that this technology could be one of the best options to reduce CO_2 levels. The currents Carbon Capture Storage (CCS) technologies are based on storing CO_2 in geological formations, either onshore or offshore.[2] This option is far from being perfect. The main problems are the unintentional leaks that may preclude the effectiveness and the life span of the storage: Indeed, it is unthinkable to stock the gas for an indefinite period; simulations show that the CCS could be a solution only if the gas can be stored for centuries[3].

Another huge challenge is the separation of the CO_2 from the other atmospheric gases. One of the solutions applied to capture the CO_2 is based on the absorption in liquid or solid media, made of amines or amino-acid solutions to form ammonium-salts or carbamates ($R_2NH + CO_2$ R_2NCO_2H); this absorption is thermally reversible. The issue of this method is the need to purify the gas before the capture process from nitrogen and sulphur oxides (NO_x and SO_x) contaminants, which are able to degrade the amine solution. This means that pure O_2 must be used to burn coal and hydrocarbons, to ideally generate only CO_2 and H_2O. This can be done only in static sites like power plants, but not for transport due to the risk linked to the pure O_2.

Consuming the CO_2 instead of storing it must be an option to consider—this can overcome the problems mentioned above. CO_2 is already used in various industries of large consumer goods, e.g. carbonate beverage and decaffeination of coffee beans in the food industry, and chemicals production (mainly used in urea, methanol and polyurethanes synthesis).[4] But the actual consumption of CO_2 is too small to be considered an effective solution to climate change.

Carbon dioxide is an unexploited resource in the chemical industry. Nowadays only a fraction of the available applications are commercially used: the direct carboxylation of molecules for the synthesis of fine chemicals or for the production of CO and other C1 chemicals. The production of the latter class of molecules containing only one atom of carbon (the more relevant are methane, methanol and formic acid) is only at the laboratory stage and quite far for being applied at commercial scale. If the direct fixation of CO_2 on useful molecules can be a long-term solution, we need to create a set of reactions scalable up to the industrial level. The production of C1 chemicals from CO_2 could be an important contribution to CO_2 utilization. Reactions that use C1 chemicals are already developed in industry, e.g., Monsanto's reaction and Fischer-Tropsch process.[4] The main challenge is the scale-up of green and economical affordable processes for CO_2 capture and conversion into C1 chemicals.

In **Figure 1.1** are exposed all the possible electrochemical reaction for the conversion of the CO_2 into a useful product.

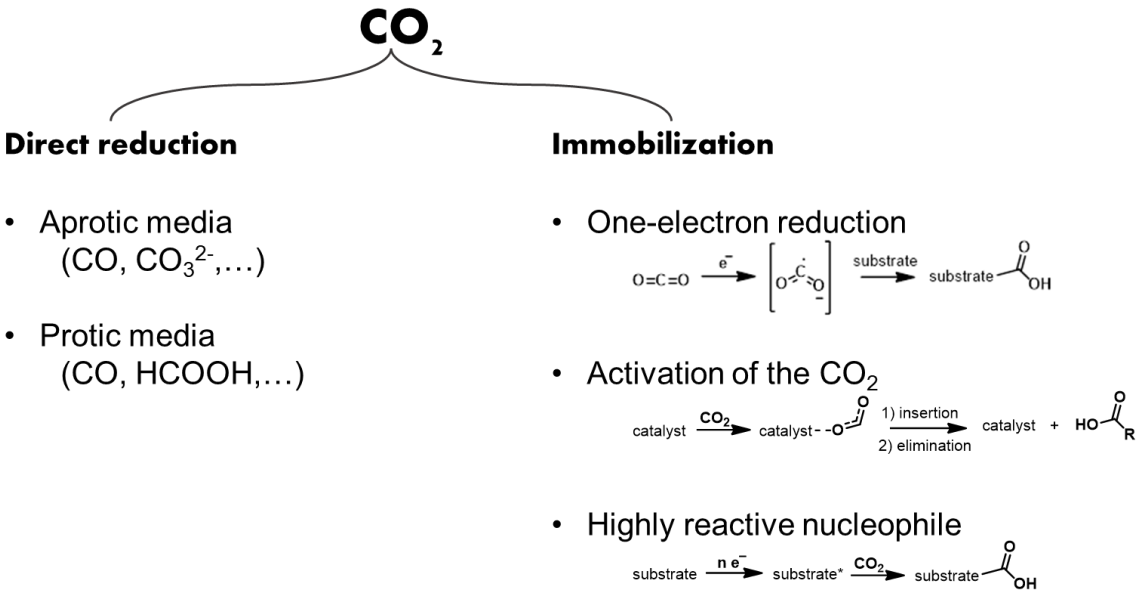

Figure 1.1 Summarize of all the reaction of the carbon dioxide to useful products. Later each of those will be exposed.

1.2 Direct electrochemical reduction of the CO_2

A green method to produce C1s from CO_2 is by electrochemical reduction, where it is possible to avoid hazardous reductive agents and directly use electrons as reagents. The CO_2 reduction pathway strongly depends on the solvent chosen. In protic solvents (typically water) or in the presence of a proton donor it is possible to obtain a large range of C1 chemicals like CO, formic acid, formaldehyde, methanol and methane (**Figure 1.2**). However, we must deal

with the reduction of the protons in solution to H_2 ($E^{'}_{H^+/H_2}$ = –0.41 vs NHE at pH 7).[5] The hydrogen evolution reaction (HER) is favoured over CO_2RR ($E^{'}_{CO_2/CO_2^{\bullet-}}$ = -1.90 vs NHE at pH 7),[6] therefore, the chosen catalyst is crucial to shift the selectivity towards the reduction of the carbon dioxide.

In an aprotic solvent with extremely low availability of protons, the mechanism changes and the product are CO, oxalate and carbonate. The key intermediate for both protic and aprotic solvents is the radical anion $CO_2^{\bullet-}$, which has the most negative potential between the various products, making the reduction of the couple CO_2/ $CO_2^{\bullet-}$ the rate-determining step in the electroreduction process since it involves a high energy species.

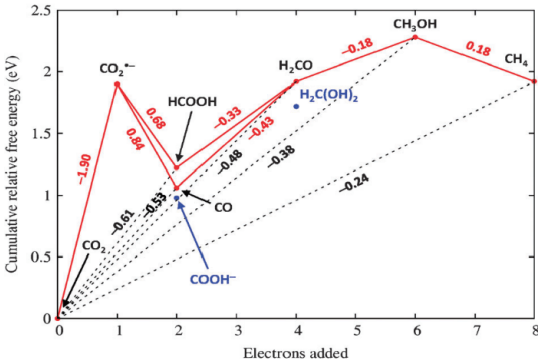

Figure 1.2 Latimer-Frost diagram for the multi-electron, multi-proton reduction of CO_2 in homogeneous aqueous solution at pH 7. [5]

In the case of an aprotic solvent, all products considered are two-electron reactions, but with different mechanisms. Theoretically, both processes (production of CO + carbonate or production of oxalate) are equally probable. Carbonate is produced by an ECE mechanism (Electrochemical-Chemical-Electrochemical step, **Figure 1.3a**), where a first one-electron reduction generates the radical anion that reacts with a molecule of CO_2, forming an intermediate radical anion that disproportionate towards carbonate and monoxide. The mechanism for the formation of the oxalate is an EC type (**Figure 1.3b**), where the radical anion undergoes a radical coupling with another CO_2 radical. The selectivity between the two pathways is highly dependent on the material of the cathode, e.g., Pb, Hg and Tl give mainly oxalate as a product while In, Sn and Au give carbon monoxide as a product.[7-9]

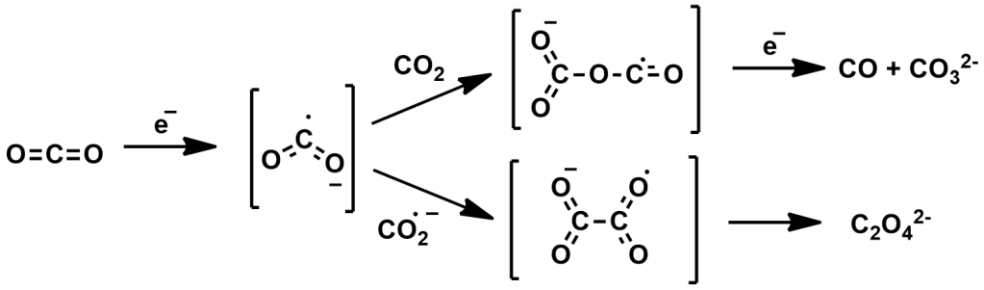

Figure 1.3 Pathway for electrochemical reduction of CO_2 in aprotic solvent. Pathway a producing CO and carbonate, pathway b gives oxalate.

The utilization of pure bulky metals as cathode materials for CO_2RR is not the best solution due to the low exploitation of the material: Only the surface is used and not the bulk, this is why metal nanoparticle supported on a suitable conductive support can offer a better surface area to volume ratio. For example, smaller metal particles have a higher fraction of surface atoms than larger metal particles. This fraction not only has an impact on the number of metal atoms that are catalytically active (metal atom utilization), but also has a substantial effect on selectivity. Furthermore, the reduction kinetics are affected by "poisoning" of the metal, adsorption of the CO_2 and desorption of the products. These processes are highly dependent on the metal's electronic structure, which is difficult to tune for a bulk pure metal. Well-designed homogeneous and heterogeneous transition metal catalysts can be used instead of pure metal cathodes can exploit as many atoms as possible and tune the selectivity by modifying the surrounding atoms.

The main categories in which the catalysts are divided are homogeneous and heterogeneous one. The homogeneous molecular catalysts are typically transition metal complexes such as Co-phthalocyanines,[10] which are able to promote the CO_2RR in common organic solvents (CH_3CN, DMF, NMP). They are less effective in aqueous solutions due to the insolubility of the catalysts. These catalysts act as a redox mediator between the electrode and the CO_2. In most cases, the real active species is electro-generated *in situ* from the complex dissolved in solution. The main disadvantage of homogeneous catalysts are the deactivation pathways affecting the long-term stability. that preclude the usage at a large scale. Notwithstanding, they are very useful to understand the CO_2RR mechanism at a fundamental level since it is possible to characterise the complex and study the catalytic process with a large variety of electrochemical and spectroscopic techniques. In addition, maybe the most important aspect is the possibility to chemically synthesize and isolate the true catalytic species involved in the catalytic cycle. A large range of molecular catalysts have been studied over time from the initial studies by Savéant and Amatore to the recent work of Isse and Sartorel. The most studied CO_2RR catalysts range from iron and cobalt porphyrins in organic media, mainly DMF

and CH_3CN, to non-heme ligands such as tetraazacyclam macrocycles, pyridyl-based macrocycles and non-macrocyclic tetradentate nitrogen ligands. For all those ligands the most studied metal centre are Fe, Co, Ni in their various oxidation states.

The alternative to homogenous catalysis is the heterogenous one, where the catalyst is casted on the surface of a collector electrode by filming a catalyst solution over a conductive support, which is typically made of a carbon material. Furthermore the catalytic site could be chemically immobilized on a conductive support for example by grafting a molecule on a graphitic surface or is a self-standing electrode bearing active site resembling those of a homogeneous catalyst. This last case is for example the one of M-N-C catalysts where the active site is a metal surrounded by four nitrogen atoms ($M-N_4$) as in metal porphyrin complexes, which will be introduced later on in this chapter. With heterogeneous catalysts, different problems of the homogeneous catalyst can be overcome, such as the solubility limitations (there are few water-soluble catalyst complexes), and the stability of the complex. For example, in M-N-C catalysts, the active site is embedded in a solid matrix (typically carbon) that limit the decomposition and enhance the stability with respect a homogeneous catalyst. Despite resolving the problematics of the homogenous catalysis, the heterogeneous catalyst brings about new factors to consider, first of all, the physicochemical interaction at the catalyst-electrode interface and the solution-catalyst interface, which may change drastically the reactivity, in turn altering the reaction pathways. Indeed, heterogeneous and homogenous catalyst, even with the same structure, cannot be directly compared. Electrode adhesion, catalyst loading and casting methods are factors not considered on homogeneous catalysis. In particular, the last two factors have a huge importance on the availability of the catalytic sites. The right loading can provide a thin layer of catalyst that cover all the surface of the electrode. On the other hand, a low loading cannot homogeneously cover the electrode whereas a high loading provides a thick film, where the inner layer cannot be reached by the solution or the film thickness might involve both ohmic resistance or severe mass transport limitation.

Heterogeneous catalysis can be prepared with a variety of structures. With the immobilization of a homogenous complex, it is possible to preserve the behaviour of the catalyst with very few changes, but poor electrochemical contact and detachment during the operation are the major limits. Various method to immobilize the catalyst are available: electropolymerization creates an electroactive polymer film with a precise control over the thickness and surface coverage, both depending on the number of voltametric cycles. A good

example of this strategy is in the work of Daasbjerg and coworker,[11] they create a film with a carbazole-functionalized iron porphyrin (FeTCPP) on different electrode surfaces, glassy carbon and indium tin oxide. Despite the excellent coverage obtained and the precise control on the film, the film has not a sufficient chemical stability for long-term use. Another strategy is to use covalent bond to attach the catalyst to the electrode, Elgroshi *et alia*[12] develop a method to easily prepare a versatile modified electrode; the surface was functionalized with terpyridine through a diazonium salt and the metal ion was complexed by a reversible metallation. Immobilization through noncovalent interaction is an interesting option, exploiting π- π interaction Blackmore *et alia* had reached a high catalyst density but a bad control on the surface functionalization, the explanation provided is that at very negative potential the pyrene used to immobilize the complex has electrostatic repulsion with the surface or it loses planarity and as a consequence the binding capability.

Reticular 3D materials, such as covalent organic frameworks (COFs) and metal-organic frameworks (MOFs), is another class of materials and the basic concept behind them is to build stable crystalline structures through building units linked through directional bonds. They can provide tuneable structure and well-defined molecular sites but are limited by the thickness of the layer grown on the electrode; this strongly influences the electron and mass transport properties of the material. Gu and coworker developed a cobalt porphyrin MOFs where the porphyrin units are linked to Zr-BTB nanosheets (BTB= 1,3,5-tris(4-carboxyphenyl)benzene) to form a 2D porous structure.[13] COFs materials are very similar to MOFs materials but they have a non-metal element such as boron or nitrogen as nodes instead of having a metal atom with organic ligands.

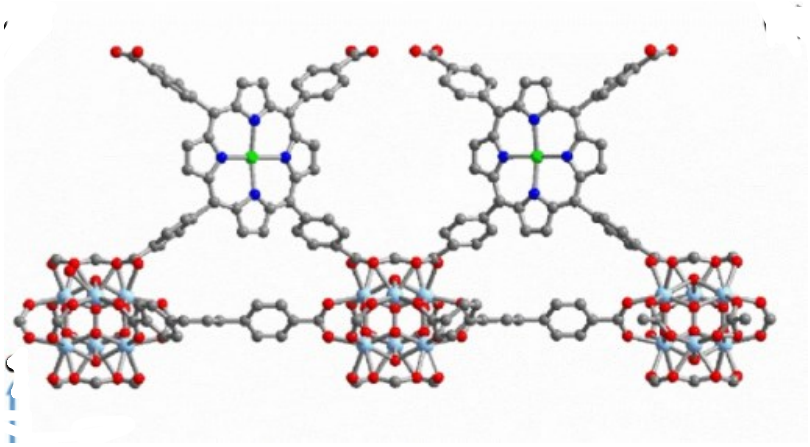

Figure 1.4 Zr-BTB MOFs studied by Gu et coworkers.

Nanostructured materials, metal clusters and metal nanoparticles (NPs), are extremely attractive due to their high surface-to-volume ratio and the presence

of reactive surface sites with low coordination number. Their activity is dependent on the size, aggregation level, shape and composition of the nanostructure. Strasser and co-workers studied size-dependent CO_2RR for Au nanoparticles, in the work they found a drastic increase in current density with decreasing NP size, along with a decrease in Faradaic selectivity toward CO.[14]

Single-atom catalysts (SACs) are an attractive class of heterogeneous catalysts, the easily synthetic steps and the tunability of the support make them a valid alternative for heterogeneous catalysis. In general SAC has embedded active sites, hetero atoms coordinated or not with a metal, on a support, a metal oxide or carbon. A large kind of single-atom catalyst are reported in literature, e.g., the Pt single atom catalyst supported on iron oxide Zhang and coworker[15] or the Cu atom coordinated to N-P-S atoms on carbon synthetized by Anouar *et alia*.[16] Their major disadvantage, compared to the other methods, is the low control on the type of active site, because during the synthetic steps a large variety of sites are produced, not only the most active one.

1.3 Electrochemical immobilization of CO_2

The carboxylation reaction is a common reaction to use the carbon dioxide without the directly reduce it. It is already used to build carboxylic acid moieties, which can be used as intermediate commodities for further synthetic applications (**Figure 1.5**) or used as-is.

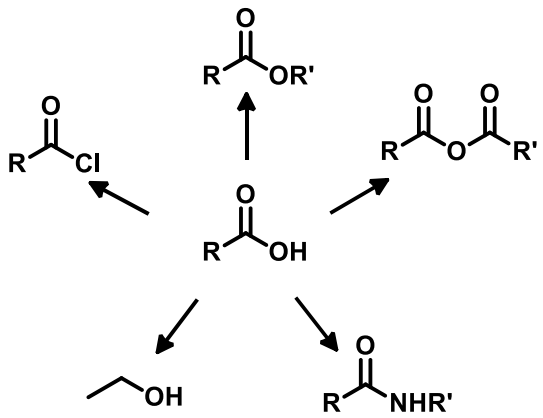

Figure 1.5 Common functionalization of a carboxylic acid.

Carboxylation reactions can be divided into three categories based on the different ways to improve the reactivity of CO_2.

i) The first category and more direct one is the one-electron reduction of the CO_2 to the radical anion, a very reactive species (**Figure 1.6**). In literature are present different works about the capture of $CO_2^{\bullet-}$, one example is the carboxylation of styrene to the respective carboxylic acid reported by Malkov and Buckey. In this work, carbon electrodes were

used as cathode, along with a non-sacrificial anode.[17] Matsuoka[18] and Jamison[19] exploited photochemistry to generate the radical anion using *p*-terphenyl as a photoredox catalyst to achieve a 100% atom economy of α-aminoacids. *p*-terphenyl was used also as photoredox catalyst in combination with 1,2,2,6,6-pentamethylpiperidine to carboxylate the styrene.[20] Despite the excellent atom economy, all the atoms of the reagents are in the products, and the simplicity of the setup. The major disadvantage in deploying these reactions is the high energy required to generate the radical anion and the lack of selectivity. Indeed, an extremely nucleophile molecule free in solution will react with every nucleophile present. Additionally, the radical anion can dimerize to form oxalate and other dicarboxylated species; for these reasons, this way is avoided, and other solutions are preferred.

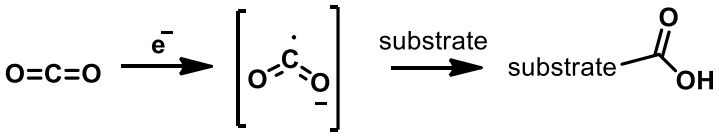

Figure 1.6 General mechanism for the direct reduction of the CO_2 to the radical anion and the successive nucleophilic attach on the substrate.

ii) The second alternative is the activation of the CO_2 using a catalyst that enhances the electrophilic reactivity of the gas (**Figure 1.7**). The activation of CO_2 typically takes place through coordination of the molecule to a catalyst, then an insertion reaction on the CO_2 takes place; the usage of a Grignard reagent with CO_2 is the first example of this kind of reactivity. Recently, elegant solutions are proposed, e.g., organoborane halides were carboxylated with CO_2 using N-heterocyclic carbene copper as catalyst as reported by Hou and coworker.[21] The general catalytic cycle of this kind of reactivity can be resumed in three steps: coordination of alkyl moieties to the metal centre, coordination of the CO_2 to the centre, these two points are not necessarily in this order, then insertion of the alkyl moiety on the carbon dioxide. The main advantage is the capability to tune the reactivity modifying the ligands. With this approach it is possible to achieve asymmetric carboxylation as shown by Hopmann at co-workers;[22] the various coordination of the CO_2 to the metal centre can be used to favour some product or different reactions.

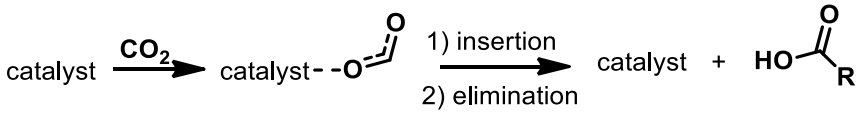

Figure 1.7 General mechanism for the activation of the CO_2 by a catalyst and the successive insertion of a nucleophile on the CO_2.

iii) The usage of molecules that can produce species able to attack the inert CO_2 are commonly used, in this work this type of reactivity was studied (**Figure 1.8**). These strategies are based on the intermediacy of alkyl anions, generated either by homolytic bond-cleavage of C-(pseudo) halide. Such intermediates are nucleophilic enough to react with carbon dioxide, König[23] and Murakami[24] works show that these strategies work even with C-H sp^3 bond. This strategy is exploited by electrochemists and photochemists with diverse methods, in electrochemistry is preferred to use a dissociative electron transfer (DET) using two electrons to produce a carbon anion, while in photochemistry is more common to use a single electron transfer (SET) to generate a radical. Those differences are due to practical reasons: in photochemistry are largely used homogeneous catalysts while in electrochemistry heterogeneous ones are preferred to homogeneous ones. With homogeneous catalysis is easy to create complexes able to act as redox shuttles of one electron reduction, in heterogeneous catalysis this is more difficult to achieve.

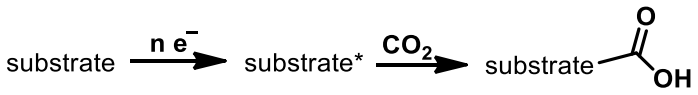

Figure 1.8 General mechanism for the activation of the substrate (substrate* = substrate activated) and the successive nucleophilic attach on the CO_2. n is the number of electrons involved, it depends on the mechanism used SET or DET.

1.3.1 Electrochemical cleavage of C-Cl bond

The cleavage of an organic halide belongs to the third category; breaking the bond between C and Cl in an organic halide is a reaction that plays an important role in organic synthesis[25] and in the field of environmental chemistry and remediation.[26] The mechanism of C-Cl electrochemical cleavage was investigated by Savéant,[27] who described two main events: the electron transfer and the bond breaking. These two events can occur stepwise (**Figure 1.9a**), with the formation of a radical anion as intermediate, or can be concerted (**Figure 1.9b**), where the ET and the bond breaking are simultaneous. For both mechanisms the determining step is the transfer of a first electron to the C-Cl bond, but from here the mechanism evolves depending on the orbital involved. In the case of a stepwise mechanism the substrate has a low lying π^* orbitals able to accept the electron, while in the case of a higher energy σ^* orbital, involved the molecule undergoes a concerted cleavage. The radical $R^\bullet$ is often more easily reducible than the parent RX molecule, especially when X = Cl or Br, so that an overall two-electron reduction wave is observed.

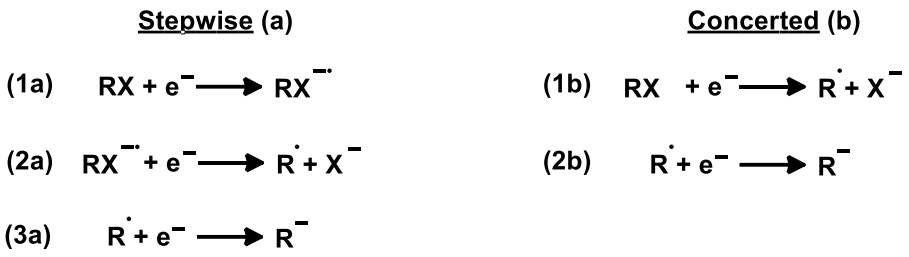

Figure 1.9 Comparison between stepwise cleavage (a) and concerted cleavage (b).

Both mechanisms fall under the important category of DET. DET provides an elegant and chemically clean way to generate reactive species such as bases or nucleophiles. In this case the resulting carbanion is an extremely reactive nucleophile that can be exploited to react with the electrophilic carbon of the carbon dioxide, a very stable and inert molecule; this is a smart way to overcome the energy requirement for the direct reduction of CO_2.

1.4 Single atomic site catalysts

Single atomic site catalysts (SASCs) are a class of heterogeneous catalysts where the catalytic sites are highly dispersed on the support; this gives advantages compared to the classic heterogeneous catalysts: first, all the sites available are exploited and it is possible to minimize the loading of the catalyst while maintaining its activity, which is important especially when rare and precious metal are used. In general, a SASC can be described as a support material with functional element (N, S, O, P, ecc.), that can change the characteristic of the material. During the synthesis support and dopant molecules with the functional elements can form ordered structures stabilizing metallic atoms; in some case these structures are the catalytic sites and mimic a homogenous catalyst adsorbed on a surface, e.g, N_4 site reassemble a porphyrin (**Figure 1.11**).

The most common supports material are carbons, such as nanotubes, carbon black and nanofibers;[28] the main advantage of these materials are the availability, ease of preparation, and the physico-chemical stability in a vast range of conditions. In order to tune physico-chemical properties, the carbon materials can be doped with heteroatoms like N, P, S or B.[29] Unlike the homogenous catalysts, the SASCs are generally obtained by thermal treatment of metal precursors (inorganic salts or complexes) and a support (heteroatom-rich organic molecules) that, depending on the synthetic conditions, give rise to isolated molecular-like surface units. These molecular-like units are the main responsible for the catalytic effects, e.g., for Oxygen Reduction Reaction (ORR) and for the CO_2 Reduction Reaction (CO_2RR).

In aqueous media the main catalytic sites are the M-N_x, in particularly the M-N_4 [30] (where M is a metal); these sites resemble a square-planar complex with porphyrin as ligand, which is the most used biomimetic catalyst—the same structure is responsible for natural processes like photosynthesis. Explorative studies on metal porphyrin complexes show the activity of these complexes towards different reaction such as ORR, CO_2RR[31] and dehalogenation of chloroalkenes[32–34]. Simplifying the structure of an M-N_4 to a porphyrin complex is a good way to rationalize the behaviour of a SASC and study its activity; indeed, iron porphyrin is used as a model study for the ORR[35]. The main problem of this simplification rises when heteroatoms are present nearby the site and not directly coordinated to the metal centre. In fact, heteroatoms change the electron density of the MN_X modifying its activity, so that it can no longer be described as a porphyrin-like complex. Instead, a more extended structure (graphene plane) needs to be considered. (**Figure 1.10**).

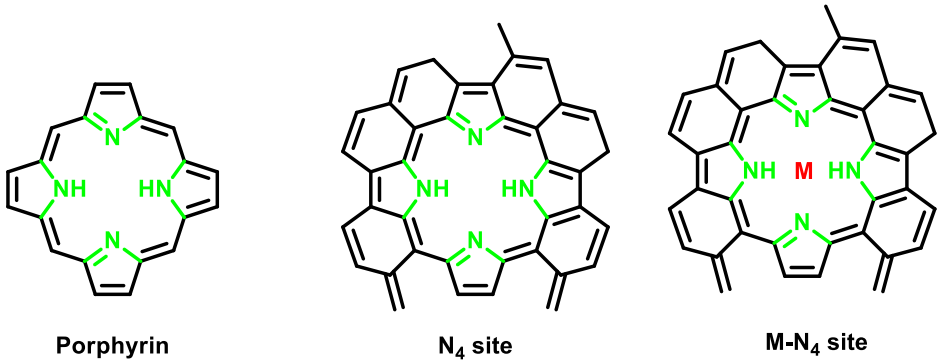

Figure 1.10 Comparison between porphyrin and N_4 site.

Despite the M-N_4 sites are the most interesting ones from a catalytic point of view, they are not the only structure present and active on the surface of a carbonaceous support; indeed, obtaining only N_4 sites is quite challenging and in most of the synthesis what is obtained is a variety of structures composed by pyrrolic N, pyridinic N and graphitic N (**Figure 1.11**) in different ratios. The coordination number of the central metal in M-N_X spans from 1 to 5.

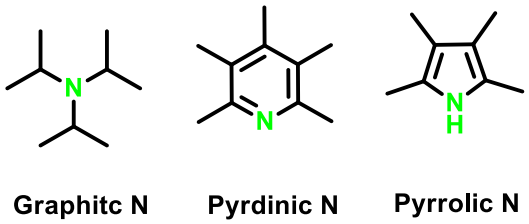

Figure 1.11 Different types of N in a SASC.

1.4.1 Metal SASCs in CO_2RR

A various range of metals can be exploited to produce SASCs for CO_2RR; nowadays, all studies are focused on earth-abundant transition metals (M = Mn, Fe, Co, Ni, Cu) in aqueous media. From the test with different MN_4 SASCs is possible to see the activity of those sites and their selectivity. This last parameter has great importance in aqueous media, where the HER can be a huge disadvantage, being a parasite reaction due to the easy reduction of water to molecular hydrogen, compared to the reduction of CO_2.

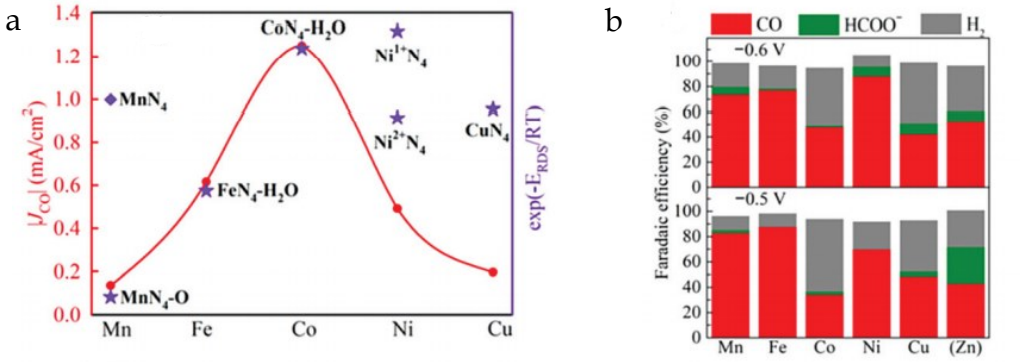

Figure 1.12 Performance of different metal SASCs. [36]

From the graph reported in **Figure 1.12** it is possible to deduce the general behaviour of the MN_4 sites. The *volcano plot*, **Figure 1.12a**, diagram shows that transitions metals from the right of the periodic table can reach higher current density (*J*) with the CoN_4 coordinated with water at the top, despite theoretical studies demonstrate that the SACS with Ni should be the most active. In **Figure 1.12b** on the left the selectivity of MN_4 moieties are displayed; Mn and Fe sites are more selective towards the CO_2 reduction products. These extremely different behaviours between the SASCs can be linked to the variation of the oxidation state of the metal and the binding energies of the key intermediates involved in the CO_2RR process. The variation of the oxidation state and the access to an "active" oxidation state are the keys processes in every catalytic process; e.g. Fe(I), is considered the active catalyst for CO_2RR in homogeneous catalysis. From the studies conducted on different metal centres arised that Fe, Ni and Cu changed their oxidation state, for Fe the oxidation number change from 3+ to 2+, for Ni from 2+ to 1+ and Cu is reduced to 0; for Mn(II) and Co(II) the oxidation state remained unchanged.

The rate-determining step (rds) in the CO_2RR can be rationalized by evaluating the binding energy of the intermediates via DFT calculations. It is possible to distinguish the SASCs in two separate categories, the ones with the desorption of the CO as rds, which is the case of FeN_4 and MnN_4 moieties, and the ones where the rds is the CO_2 activation and first electron transfer (ET). NiN_4 and CuN_4 fall in this category. CoN_4 is the only catalyst not presenting a

clear rate-determining step: the desorption of CO and the activation of CO_2 contribution balance each other, which gives this catalyst the highest reactivity among the investigated ones.

SASCs are rarely investigated in organic solvents. Recently a CuN SASC was used by Zheng and coworkers[37] in anhydrous acetonitrile for the direct carboxylation of the styrene via formation of the CO_2 radical anion. Zheng and coworkers achieved good yields towards phenylsuccinic acid and a low faradic efficiency toward C1 chemicals (the sum of CO and CH_4). The valence state of Cu was between +1 and +2 and quite different from what was observed in water, as discussed above, where the Cu during the CO_2RR is reduced to oxidation number 0.

1.4.2 Metal SASCs for dehalogenation

There are few examples of metal SASC for the cleavage of the C-Cl bond, the major studies are focused on the despondency of volatile organic compounds (VOCs) in particularly dichloroalkenes.[33,34,38,39] The studies of Gan et alia [34,38] on 1,2- dichloroethane (DCE) shows that the most active site for the cleavage of the bond C-Cl is the FeN_4, and the N 2p site but depending on the electronegativity of the site. The N site with more positive N 2p states, such as graphitic N and oxidized N, are prone to produce CH_2CH_2 from DCE, meanwhile the production of $CHClCH_2$ from CH_2ClCH_2Cl dechlorination tends to occur at the N site with more negative N 2p states such as pyridinic N and pyrrolic N sites. Based on these results, a possible dechlorination mechanism of DCE on the oxidized N site was proposed.

1.5 Purpose of the thesis

The project described in this thesis considers to investigate the electrocatalytic behaviour of FeN_4 active site embedded in carbon materials in an organic media such as acetonitrile. There are plenty of examples in literature of M-N-C electrocatalytic activity for oxygen reduction or CO_2 reduction, but surprisingly there are no example of their activity in organic solvents. The reaction chosen for testing the SASCs are two:

- The CO_2RR, due to the topicality of the theme and to the high solubility of the gas in acetonitrile (0.282 M[40]).
- The electrochemical cleavage of the C-Cl bond. This was chosen because is a well-known reaction and the mechanism is simple and deeply studied, and it allows to perform a series of electrochemically induced activation of nucleophile reactions versus for example CO_2 as in electocarboxylation reaction.

2 Experimental procedure

2.1 Instruments and techniques

2.1.1 Electrochemical measures setup

Biologic SP300 was used for the electrochemical characterisation adopting a three electrodes setup: a glassy carbon (ø=5.5mm) as working electrode, the reference electrode was an Ag/AgCl wire in a solution of DMF/acetonitrile (3:1) saturated with $(Et)_4NCl$, the counter-electrode was a graphite rod. A six-neck electrochemical cell was used. A mass flow controller Matheson Mod. MFB-21 was used to control the concentration of CO_2. The working electrodes were prepared polishing them with a micrometric polish pad and three kind of diamond paste (3 µm, 1 µm and 0.25 µm), after each paste the electrode was sonicated in ethanol for 5 minutes.

The materials were deposited on glassy carbon electrodes for studying the electrochemical behaviour. The drop-casting technique was chosen as casting procedure due to the extreme simplicity and velocity; it involves dropping a known amount of an ink, containing a certain quantity of catalysts, namely of known concentration, on the surface of the electrode and then let the solvent evaporate. An ink was formulated with this composition: chitosan (binder) at 7% of the total mass of the carbons, catalyst and Ketjenblack EC-300J carbon in ratio 9:1, the solvent chosen is a mix of water and DMF (95:5 in volume).

The deposit on the electrode had a density of 0.6mg cm^{-2}.

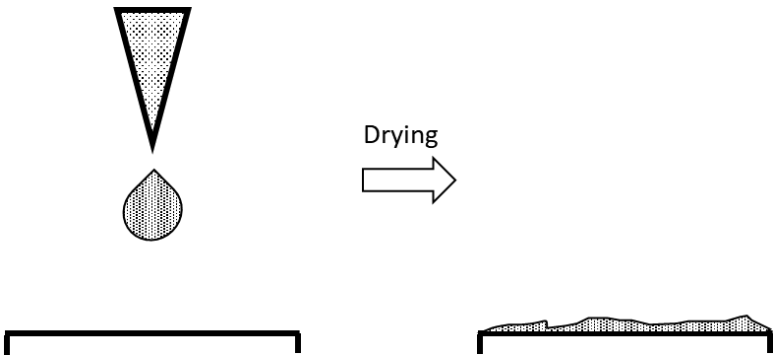

Figure 2.1 Drop casting technique.

2.1.2 Electrolysis setup

EG&G Parc Potentiostat/Galvanostat Model 273A was used for electrolysis experiments. For electrolysis a divided cell with a Pt mesh as counter-electrode was used, the separator was a G2 glass frit with Agar gel saturated with electrolyte. An Ag/AgCl wire in a solution of DMF/acetonitrile (3:1) saturated

with $(Et)_4NCl$ and a carbon paper sheet were adopted as reference and working electrode, respectively. The change of potentiostat for the electrolysis was necessary since there are high voltage between the working and the counter electrodes, mainly caused by the resistance of the junction of counter-electrode (glass frit + Agar gel). The working electrode used was 1.5cm x 1cm with a deposit density of 0.3mg cm^{-2}.

Catalyst deposition on working electrode was performed by spray coating. An aerograph was used to spray the ink in a homogenous layer of the ink with the same formulation used for the drop-casting, to speed up the process a thermal gun was placed above the carbon paper to dry the solvent.

The reason for this technique in place of using a drop-casting approach is due to the large surface to cover. Spray coating allows a better and more homogeneous coverage than drop casting when high surface area need to be covered, with the only drawback that much more catalyst ink needs to be prepared and consumed. Also, the surface of carbon paper is hydrophobic which make difficult to perform a drop casting with aqueous ink. The ink was sprayed in several portions and after each aliquot, the surface is let dry completely; the carbon paper was kept hot with a thermal gun, in this way the layer formed upon it is very homogenous.

Figure 2.2 Spray coating technique.

2.1.3 HPLC analysis

The HPLC (High-Pressure Liquid Chromatography) technique was chosen to analyse the liquid products. This technique allows to separate different compounds depending on their interaction with the eluent (the mobile phase) and the packed material in the column (the stationary phase). The interaction between the compound and the phases depends on its polarity, in this case a reversed-phase column was used. Therefore, the stationary phase is non-polar, which means that the more the polarity of the molecule to analyse the lower the retention time, i.e., the time employed by the compound to be eluted out of the column. The solution to analyse was injected with a syringe previously rinsed three times with the solution to analyse, then pumped at high pressures, in the order of tens MPa, through the column and then to the detector. The

instrument used is a Jasco PU-2080 coupled to an in-line degasser Jasco DG-2080-53, it helps to avoid the formation of bubbles that can disturb the measurement. The column used is a C18 reversed-phase, the Synergi 4µm Hydro-RP 80Å, LC column 250x4.6mm, with a guard column to protect it. The detector used is the UV-Vis detector Jasco UV-2075 Plus mounted in-line at the end of the column. The eluent chosen for the runs was a mix between acetonitrile and water (60:40 in volume).

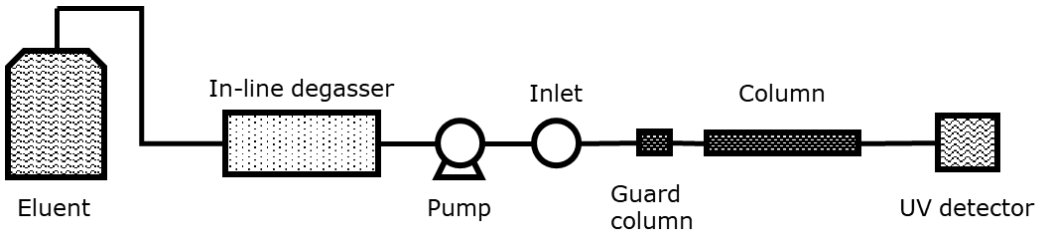

Figure 2.3 HPLC instrument.

2.1.4 GC-TCD analysis

A gas chromatography (GC) technique coupled to a thermal conductivity detector (TCD) was used to analyse the gaseous fraction of the products. Argon was used as gas carrier. Similar to a HPLC, the GC let to separate the different volatile molecules on the interaction between mobile phase and stationary phase. In this case two column was used to separate the products, a J&W HP-PLOT Q capillary GC column in fused silica, 30 m, 0.32 mm, 20.00 µm, 5 inch cage (**Column 1**) and a J&W HP-PLOT Molesieve GC column in fused silica, 30 m, 0.32 mm, 25.00 µm, 7 inch cage (**Column 2**); the usage of a second column is necessary due to the impossibility to separate small molecule, like CO, N_2, H_2 and O_2 in the first column, but **Column 2** can deteriorate if large molecule, like CO_2 and H_2O, goes in. Therefore the chromatographic run was performed using the following program: after the run start, the gases to analyse enter in **Column 1**, where large molecule are detained, and the valve that connect the two columns is opened for 2.7 minutes. During this time, the molecules not retained by **Column 1** entered in **Column 2**, (the flux is 3.5 mL/min). After 2.7 minutes the valve is closed to avoid the clogging of **Column 2** with large molecule. At this point, **Column 1** is directly connected to the detector and the flux in **Column 2** is 3 mL/min. After 4 minutes the valve is re-opened and the flux bring up to 15 mL/min to optimize the separation in the molecule sieves. At 7 minute starts a ramp from 50 °C to 120°C at a rate of 10°C/min, this is necessary to purge CO from **Column 2**. At 10 minutes the valve switch and close the connection between the two columns linking **Column 1** directly to the detector. At 15 minutes the run ends.

The detector used was the Agilent G4407A Thermal Conductivity Detector, consisting of an electrically heated filament in a temperature-controlled cell, which senses changes in the thermal conductivity of the column eluent and compares it to a reference flow of carrier gas. Under normal conditions there is a stable heat flow from the filament to the detector body, when an analyte elutes and the thermal conductivity of the column effluent is reduced, the filament heats up and changes resistance. This resistance change is sensed by a Wheatstone bridge circuit which produces a measurable voltage change. The column effluent flows over one of the resistors while the reference flow is over a second resistor in the four-resistor circuit. Since all compounds, organic and inorganic, have a thermal conductivity different from helium or hydrogen, virtually all compounds can be detected.

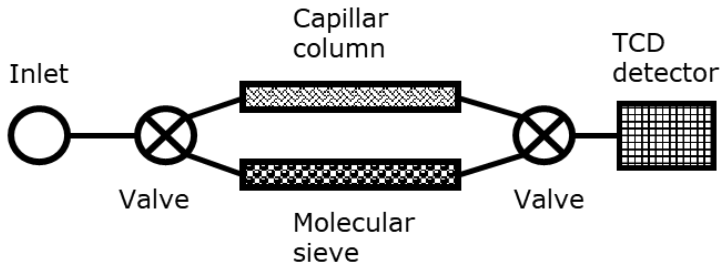

Figure 2.4 GC-TCD instrument.

2.2 Reagents

Acetonitrile HPLC grade was distilled under CaH_2 and stored under an inert atmosphere to maintain it anhydrous. $(CH_3CH_2)_4N^+BF_4^-$ was recrystallized with ethanol and stored in a dryer. CO_2 and Ar were used as purchased by AirLiquid. The benzyl chloride, chloroacetonitrile and their respective carboxylic acid were used as purchased. Ketjenblack EC-300J and carbon black Super P are used as carbonaceous supports.

2.2.1 Distillation of acetonitrile

The distillation of the acetonitrile was made using a distiller under inert atmosphere of N_2. A flux of N_2 was passed into the distiller to eliminate the moisture. After the solution of acetonitrile was bring to boiling point and keep it for 12h to activate the CaH_2 in solution and anhydrify the solvent. The solvent was distilled at a slow rate and the head of the distillation was eliminated (approximately the first 30 minute of distillate after the vapours reached the condenser), this avoid the presence of impurities due to the reaction between acetonitrile CaH_2 and $Ca(OH)_2$, the last one was produced by reaction between calcium hydride and the water.

2.2.2 Materials

All the three reported materials were previously studied for the ORR in aqueous electrolyte.[41,42]

- FNCBCO2

The starting material for the used catalyst is iron (II) *tris*-(1,10-phenanthroline) chloride and carbon black (CB, Super-P) pre-treated thermally in a CO_2 atmosphere[17]. The synthesis requires three steps: the first is a thermal treatment in a controlled atmosphere, where the precursors are placed in a tubular furnace in a ratio of 2%mol of complex respect to the carbonaceous support with an initial flux of N_2 of 25 cm^3/min for 1h at ambient temperature to eliminate oxygen, then a ramp to 100°C and maintained for 1h to eliminate water, at this point the flux is changed to 23 cm^3/min of N_2 and 2 cm^3/min of H_2 and start a ramp to a temperature of 900°C which is maintain for 2h. Eventually, the furnace was cooled to ambient temperature. After the thermal step, an acid leaching of the raw material with 1M of H_2SO_4 at 100°C for 3h was performed to eliminate the impurities created during the thermal treatment (iron carbide, metallic iron, iron oxides), as final step the thermal treatment is repeated.

- PAJ

Is a commercial product under the name PMF-011904 from Pajarito Powder Inc. This catalysts is a material synthesized via hard templating with fumed silica, using the Varipore™ process[43],. The catalyst was used as received.

- CNRS

The material is a ZIF-derived catalyst from CNRS/University of Montpellier[44]. The catalyst was used as found.

2.3 Measurement techniques

The performance of the catalyst was analysed with electrochemical techniques, cyclic voltammetry (CV) and electrolysis.

2.3.1 Cyclic voltammetry

The cyclic voltammetry is a transient technique that measures the current with respect to the potential applied. The potential is changed during the experiment to scan a determinate range. In **Figure 2.5** it is showed the variation of the potential with the time, from a starting point (E_i) the potential is increase to an inversion potential (E_{inv}), chosen by the operator, then it goes back to the starting potential; during the scan the current is recorded.

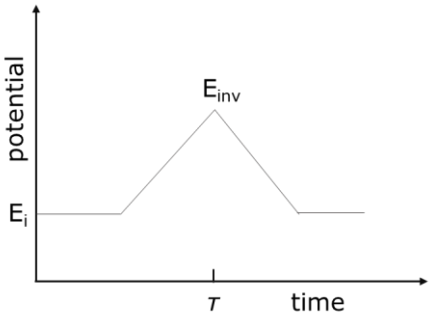

$(0<t \leq \tau)$ $E=E_i-vt$

$(t>\tau)$ $E= E_i-2v\tau+vt$

Figure 2.5 and Eq 2.1

Figure 2.5 Plot of how the potential change over the time. **Equation 2.1** This system of equations describes how the potential change in a cyclovoltammetry during time.

The typical *i-E* plot for this system is the one in **Figure 2.6**, nicely called "duck shape". From the plot can be extracted the diagnostic parameters for this system: peak currents (i_p), peak potentials (E_p) and their mathematical manipulation. In this kind of system, the peak current is dependent from the scan rate **Equation 2.2** but the ratio between the anodic peak current and the cathodic peak current is 1.

- Reversible system

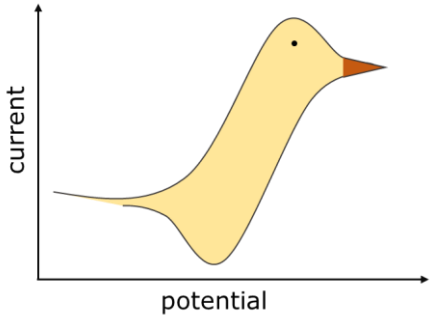

$O+ne^- \rightleftarrows R$

Figure 2.6 Typical "duck shape" cyclovoltammetry of a reversible system.

The typical *i-E* plot for this system is the one in **Figure 2.6**, nicely called "duck shape". From the plot can be extracted the diagnostic parameters for this system: peak currents (i_p), peak potentials (E_p) and their mathematical manipulation. In this kind of system, the peak current is dependent from the scan rate **Equation 2.2** but the ratio between the anodic peak current and the cathodic peak current is 1.

$$i_p=0.446nFAC\sqrt{\frac{nFvD}{RT}} \qquad \textbf{Equation 2.2}$$

Equation 2.2 The Randles-Sevcik equation for the reversible system where n is the number of electrons, F is the Faraday constant, A the area of the electrode, C is the concentration of the specie, v the scan rate, D the diffusion coefficient.

The peak potentials are independent from the scan rate, in fact they depend only on thermodynamic constants; the separation between anodic and cathodic peak is constant and also the separation between one peak and the

half peak is constant, deviation from this behaviour is a diagnostic criterion to suspect irreversible process, chemical or electrochemical ones.

$$E_p = E_{1/2}{}^{*} - 1.109\frac{RT}{n^2F} \qquad \textbf{Eq2.3a}$$

$$\left|E_p - E_{p/2}\right| = \frac{56.5\ mV}{n} \qquad \textbf{Eq2.3b}$$

Equation 2.3 Equation 2.5a describes the peak potential in an reversible system, it depends on from constants. Equation 2.5b describes the separation between the peak potential and the half peak potential in a reversible system.

- Irreversible system

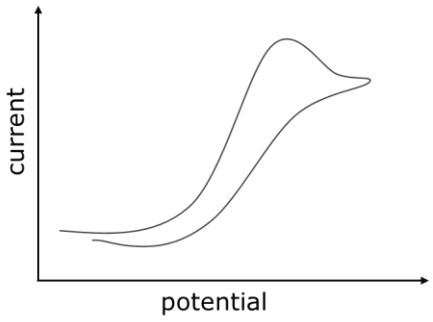

$O+ne^{-}\rightarrow R$

Figure 2.7 Typical cyclovoltammetry for an irreversible system.

In this case the *i-E* plot acquire a single wave shape. The peak potential now is dependent on the scan rate, it is no longer constant, and the peak current is described by the same equation for reversible systems, but with a different coefficient.

$$i_p = 0.496nFAC\sqrt{\frac{nFvD}{RT}} \qquad \textbf{Equation 2.4}$$

Equation 2.4 The Randles-Sevcik equation for irreversible system.

In irreversible systems the peak potential is not a constant, but it depends on the scan rate, see **Equation 2.5a**. From the peaks potentials at various scan rates can be determinate the charge transfer coefficient α which is an important parameter for kinetic studies, e.g., in dissociative electron transfer the value of α can discriminate between a stepwise mechanism (α >0.5) and a concerted one (α<0.5). α is a potential dependent factor that measure the symmetry of the energetic barrier of an electron transfer and it has a value between 0 and 1.

---

* $E_{1/2}$ is the half-wave potential. It is an estimation of the standard potential (E^0) of the specie for reals system, reversible or irreversible ones, and it is described by the Nernst equation $E_{1/2} = E^0 - \frac{RT}{nF} ln \frac{a_{rx}}{a_{ox}}$.
For further information see this article[45]

$$E_p = E_{1/2} - 0.78\frac{RT}{nF} + \frac{RT}{nF}\ln\frac{kRT}{vnF} \qquad \textbf{Equation 2.5a}$$

$$\frac{dE_p}{d\log} = -\frac{29.6\ mV}{\alpha n} \qquad \textbf{Equation 2.5b}$$

Equation 2.5 Equation 2.5a describes the dependence of the peak potential in an irreversible system from the scan rate, v. The parameter k is the kinetic constant of the reaction. From Equation 2.5b the is possible to understand how, from the different values of E_p at different scan rates, can be estimated the value of α

2.3.2 Electrolysis

Electrolysis is a technique that uses direct electric current to drive an otherwise non-spontaneous chemical reaction. The fundamental laws for this technique are Faraday's laws for electrolysis that relate the current passed through the electrode with the specie in solution consumed/produced.

$$Q = \int_0^t i(\tau)d\tau \qquad \textbf{Equation 2.6}$$

Equation 2.6 First Faraday's law of electrolysis.

The first law, **Equation 2.6**, states that the total charge passed, Q, during the period of time, t, is equal to the function of the current, $i(\tau)$, over time, in case of constant current can be simplified as **Equation 2.7**.

$$Q = it \qquad \textbf{Equation 2.7}$$

Equation 2.7 Simplification of Equation 2.6.

The second law relates the charge to the quantity of substance.

$$moles = \frac{Q}{nF} \qquad \textbf{Equation 2.8}$$

Equation 2.8 Second Faraday's law of electrolysis.

There are two kinds of electrolysis: potentiostatic, where at a fixed potential the change of the current is recorded, and galvanostatic, where at a fixed current the change of the potential is recorded.

2.3.3 Nitrite reduction stripping

This method calculates the number of active sites effectively reachable by the reagents, some sites can not be active because are too deep in the film. This work takes for granted, at least at this stage, that the active sites the FeN_4,[46] are those responsible for CO_2RR not only in aqueous solution as already

demonstrated in literature, but also in organic electrolyte. The material is poisoned with a solution of 125mM of $NaNO_2$ for 5 min at the OCP with a rotating disk electrode (RDE) set at 300 rpm. At this point the material is poisoned, the iron sites are bonded to nitrite, cyclic voltammetry in rotation is performed (5mV s^{-1}, 1600 rpm). From the CV recorded the charge associate at the NO stripping is recovered (Q) and using the **Equation 2.9** the site density normalized (SD_{mass}) to the mass is calculated. The process takes 5 electrons for each site, further details are in this article.[41]

$$SD_{mass} = \frac{Q^* N_A}{n^*F^*m} \qquad \textbf{Equation 2.9}$$

Equation 2.9 Formula for the SD_{mass}, where N_A is the Avogadro's number, n is the number of electrons associated at the stripping and m is the mass of the catalyst on the film.

3 Results and discussion

3.1 Formulation of the ink

To characterize a SASC it needs to be deposited on an electrode collector. The deposit was made with a drop-casting technique, a fast and easy technique, even if not always reproducibile.[47] In literature it was not found any specific formula for ink that works in organic media, so several ink formulations were investigated. It was necessary to formulate an ink to disperse the material to drop-cast; two components were investigated: the solvent and the polymeric binder. The solvent must guarantee a good dispersion of the powder material, which improves the reproducibility, while the polymeric binder helps to tie the catalyst to the surface of the electrode. The binder must resist on the experimental condition, in this case working at a very negative voltage in organic media. This means that in the case of gas evolution, the film must be bonded to the surface to avoid detachment and variation of catalyst's loading during the measurement.

A trial with ink without binder was attempted but was not successful. The film collapsed when the electrode was immersed in acetonitrile. Therefore, three binders were tested with this methodology: Nafion, agar gel, and chitosan (see below). In a first trial the binder was loaded at 10% in weight with respect to the total mass of the material, and in case of success the load would be lowered. Less binder generally means lower resistance of the layer. However, also very high binder loading can produce fake responses. The test was a sequence of cyclovoltammetry to high negative voltage (-2.5V vs Ag\AgCl) in CO_2 saturated acetonitrile while observing the behaviour of the film.

Nafion was the first binder tried. Nafion is a sulfonated tetrafluoroethylene-based fluoropolymer-copolymer largely used to prepare inks in aqueous media, and the principal component of proton exchange membrane fuel cell. The performances of the catalyst film were not reproducible and satisfactory, since the current decreased cycle after cycle. This was clearly related to the film detachment, indeed in solution particles was observed fluctuating.

The second tried binder was the agar gel, prepared dissolving 0.2 g of Tylosium in 20 mL of DMF. It was chosen because it is commonly used as a separator membrane in organic media. The test performed revealed that the layer is not able to resist at high voltage, in fact after the first cycle the film started to detach from the electrode surface and the current peak of the CO_2 starts to lower, as observed for Nafion.

The third binder tried was chitosan, a linear polysaccharide composed of randomly distributed β-(1→4)-linked D-glucosamine and N-acetyl-D-glucosamine recover from crustacean shells. Having passed the test in the most concentrated composition, chitosan was switched to compositions with smaller chitosan concentrations. The final loading of chitosan was 7% w/w respect to all mass of the material, a compromise between electric and physical resistance.

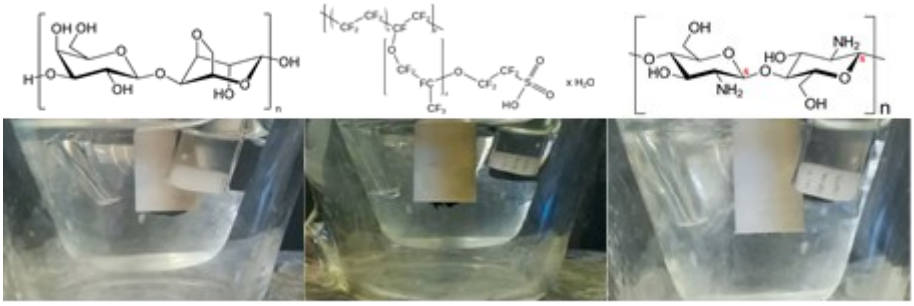

Figure 3.1 Visual of the film with the different binders after ten cyclic voltammetries to -2.5 V vs Ag/AgCl. From the left: agar, Nafion and chitosan.

One of the main problems faced with the usage of the chitosan as a binder is its solubility: it is soluble only in an acetic acid aqueous solution (1% w/w), therefore the solvent cannot be optimized to minimize the Marangoni effect (see 6.1). The Maragoni effect is responsible for a poorly reproducible deposit on the surface of the electrode. The ink was made only in water in order to avoid the precipitation of the binder. Therefore, only a very low quantity of an organic solvent (DMF) was used.

The procedure for making the ink was: firstly, the material was weighted and dispersed in the solvent, the material is composed of two components the catalyst and a low quantity of highly conductive carbon (Ketjenblack EC-300J). The Ketjen was used as a strategy to limit the resistance given by the binder, the quantity of this carbon was 10% w/w respect to all mass of the material. Secondly, the solvent was added to obtain a concentration of about 0.7 g/mL and finally the chitosan solution was added. The obtained solution was sonicated in a bath sonicator for at least 1 h to obtain a good dispersion of the catalyst.

3.2 CO_2: direct reduction on SACS

As introduced before in order to understand the catalysis of SASC in an organic solvent for the reduction of CO_2, catalysts with different properties were chosen. The catalysts studied were FNCBCO2, CNRS, PAJ (see **Table 3.1**) and a glassy carbon that was the non-catalytic electrode, chosen as reference system, on which they were deposited.

These catalysts have been already tested for the ORR reaction in aqueous media and were found to be good catalysts (faradic efficiency > 90% at -0.45 V vs RHE).[36] The behaviour of the catalysts in the ORR was taken as prediction tool for gauging the reactivity of the SASC toward the CO_2RR. Despite the huge difference between ORR and CO_2RR, this assumption was made because for both reactions the FeN_4 site is the most active one in aqueous media.

Table 3.1 Summary of the main characteristic of the SASCs used. The data are taken from this article.[42]

	FeN_x sites (%)	**SD_{mass}[b] (10^{19} sites g^{-1})**
PAJ	7.10	0.25
CNRS	15.8	1.44
$FNCBCO_2$	17.3	0.24

[a] percentage calculated with respect to the total nitrogen content; [b] the SD_{mass} was calculated by nitrite reduction stripping

The FeN_x sites percentage, determined by XPS analysis, and the gravimetric site density, calculated using the NO stripping method, were chosen for rationalising the catalytic performance of these three SASC. The FeN_x data provide the quantity of all possible sites present in the material, superficial and bulk ones, but does not tell anything about their reactivity and activity.

The SD_{mass} provides information about the sites involved in the electrochemical process. In fact, not all the sites measured by XPS can be active or involved in the catalytic process because, for example, they are not reached by the reagent when too deep in the material. Furthermore, the XPS techniques is by itself not resolutive for a precise determination of FeN_x sites in particular for low N content.

Now two probable scenarios based on **Table 3.1** can be faced:

Scenario 1

Based on the value of FeN_x sites, the reactivity of the catalysts towards the CO_2RR must follow this sequence $FNCBCO_2$>CNRS>PAJ. For high values of FeN_x is more probable to find a high number of FeN_4 sites, the most active ones for CO_2RR in aqueous media.

Scenario 2

Based on the value of SD_{mass}, the sequence must be CNRS>PAJ≥ $FNCBCO_2$. A high number of active sites is more important than the type of the sites and this suggests that the reactivity of the FeN_4 sites is different from the one seen in aqueous media.

The parameter used in this work to evaluate the activity of each SASC is the peak potential (E_p) recorded for the reduction of CO_2 in CH_3CN, which tells how much energy the system needs to reduce the CO_2, namely the more positive the E_p the lower the overpotential for the reduction of CO_2. **Figure 3.2** reports the variation of the E_p with the scan rate. From these results, none of the two scenarios exposed is fulfilled, in fact, the activity of the SASC follows the sequence $FNCBCO_2$>PAJ>CNRS. The observed behaviour is not in agreement with the trends described before, meaning that the behaviour of the Fe-N-C material in the CO_2RR in organic solution might not solely depends on FeNx active sites. Actually, it seems that the FeN_4 site is not the most active one at all. Various hypotheses to explain this behaviour can be made. Maybe other kinds of sites start to be competitive towards the reduction, this can be caused by two things: a completely different initial state of the FeN_4 site and a possible poisoning of the FeN_4 by a reagent, solvent or intermediate.

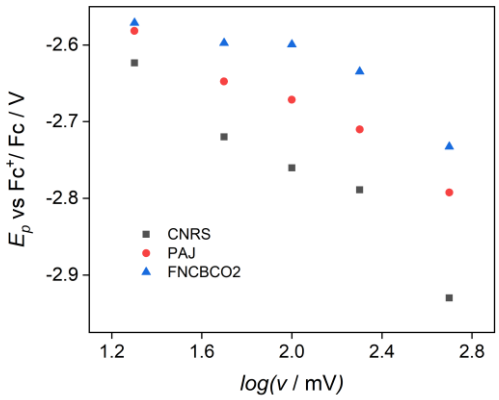

Figure 3.2 Comparison between the catalysts at increasing scan rate made in CH_3CN 0.1M $TEABF_4$ CO_2 saturated.

The hypothesis of a different initial state rises from the solvent used, acetonitrile, compared to the one used in literature, water. Viewing the site like a Fe(II) complex with an N-tetradentate cyclic ligand can help to rationalize the influence of the solvent on the site **(Figure 3.3**). At least one site is available for coordination, the site of the complex that "faces" the solution. In this axial position, the solvent is coordinated to the metal centre, the strength of coordination depends on the solvent. From the spectrochemical series rises that the water is a weaker ligand than acetonitrile, meaning the interaction between acetonitrile and metal centre is stronger than the one with water. The break of this coordination is the first step to overcome, the metal centre must have an available coordination site to bond a CO_2 molecule, but the only one available is already coordinated to the solvent; this process can be compared to a dissociative mechanism of a complex at 16 e^-.

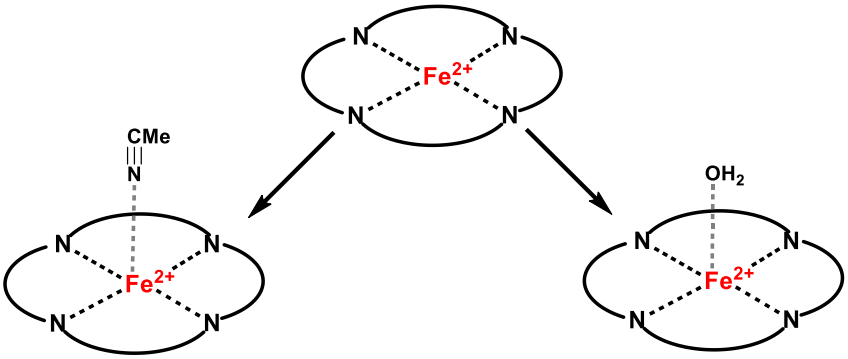

Figure 3.3 On the left the iron coordinated to the acetonitrile, on the right the iron coordinated to a molecule of water. Both reassemble a square pyramidal complex.

Another hypothesis can be formulated upon the computational studies made for the CO_2RR at FeN_4 site in water, that proceeds with the formation of CO as a reaction intermediate.[48] In this case the rate-determining step should be the desorption of the CO produced. This could be the rate-determining step even in acetonitrile but amplified because in acetonitrile CO is insoluble compared to in aqueous media. The interaction between CO and the site can play an important role and compete with the formation of the solvation sphere on CO. To confirm or exclude this last hypothesis, an electrochemical test in the presence of a CO atmosphere was made. Firstly, CO was bubbled in the cell and a scan in anodic range was performed, then cell was saturated with CO_2 and a scan in the cathodic range was recorded. The expectation is a sensitive decrease of activity if the gas is indeed adsorbed in the sites. Furthermore, a concomitant desorption peak in the anodic scan should be detected. None of those two clues of poisoning by the CO appeared.

To indagate better the behaviour of these classes of catalyst in an organic solvent, FNCBCO2 was chosen since appeared to be the most active one. Firstly, the various synthetic steps of FNCBCO2 were studied, namely the catalyst after first heating treatment (1T), after acid washing (TA) and after second treatment (FNCBCO2). Also the same SASC without the iron centre was tested.

These experiments were made to see if the various process of the synthesis of FNCBCO2 can influence its behaviour and see if the presence of the metal plays a role in the reduction of carbon dioxide or not. Comparing the various synthetic steps of the catalyst could help to understand if the FeNx sites can be important for the catalysis or some other functional group that came out from the various steps can be considered more relevant for the CO_2 reduction.

The forms of iron other than FeNx formed during the synthesis are mainly two, the firsts are metallic iron or iron carbide and iron oxides. These iron species form during the first synthetic step. at 900°C in an atmosphere of H_2,

from the degradation of the Fe (II) complex. Those iron species are completely or for the most part eliminated by the acid work-up, but this can attach sulfonic moieties to the surface of the carbon. Sulfur functional groups are the second type of active sites that can modify the catalytic process. However, the last thermal step should eliminate the sulfonic moieties leaving only the FeN_x site on the surface, this step also improves the graphitization of the material enhanced the conductivity.

From the graph reported (**Figure 3.4**) is clear that there is a variation on the catalysis between the different synthetic steps, meaning the presence of other forms of iron or sulfonic groups attached to the carbon surface affect the catalyst. The comparison made in **Figure 3.4** brings some interesting aspects, the graph shows that the catalyst with only N sites (NOFe) is as active as the one with FeN_x sites. This result is quite outstanding if we consider that in aqueous media the FeN_x sites have greater relevance than the N sites only. Recalling the hypothesis made above, where the low activity of the FeN was attributed to a "poisoning" of the site, it is possible to state that the iron is somehow "inactivated".

The sample 1T, which correspond to the catalyst with only the first thermal treatment, has comparable catalysis to the FNCBCO2. The TA, the catalyst with the first thermal treatment and acid leaching, seems to be more active with respect to the FNCBCO2, the sulfonic moieties attached after the step in sulfuric acid can enhance the catalysis at low scan rates.

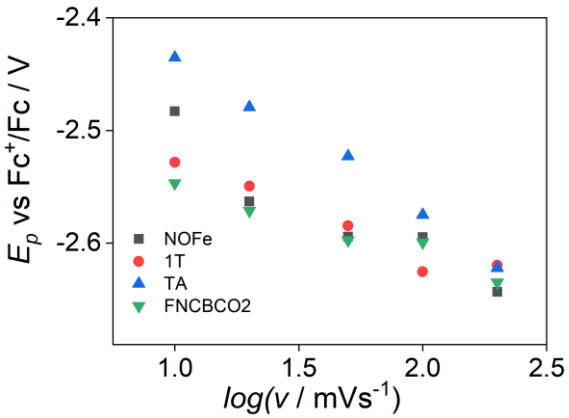

Figure 3.4 Comparison between the various synthetic steps at increasing scan rate made in CH_3CN 0.1M $TEABF_4$ with 0.1M of CO_2.

Therefore, it appears that FeN_x sites do not have a huge importance in the reduction of carbon dioxide in organic electrolyte. If FNCBCO2 is compared with the respective SASC without the iron centre, NOFe, there is not an evident advantage of one over the other. From literature seems that even the different types of N sites can promote the CO_2RR. Therefore, we investigated

whether there is a correlation between the types of N and the E_p, where the type and amount of nitrogen functional group is again determined by XPS from the deconvolution of the N 1s peak. Each SASCs tested to have a different amount of N, see **Table 3.2**.

Table 3.2 Atomic percentual of the various N types recover by N 1s deconvolution of XPS measurements.[41,42]

	N 1s	Imine	Pyridinic	NxFe	Pyrrolic	Graphitic	N-O
PAJ	2.3	14.4	11.6	7.1	39.4	22.1	5.4
CNRS	2.15	18.6	21.6	15.8	25.9	16.2	19
FNCBCO$_2$	0.59	19.8	27.2	17.3	30.3	5.4	0

For each catalyst were plotted the atomic percentual of **Table 3.2** against the E_p but a clear correlation was not found. The identification of a plausible and alternative catalytic site to the FeN_x sites is not trivial from the sole data recovered.

The next step was to compare the catalytic performance of the SASC with respect to a non-catalytic electrode, inert towards the CO_2RR, and measure the variation of the E_p between the the two types of electrodes. The choice was to adopt the glassy carbon, which is commonly used as an inert and smooth electrode, and because of that it is considered to be the best approximation to a source of outer-sphere electron transfer. The first set of data (**Figure 3.6**) seems to show electrodes with the SASC having a catalytic behaviour towards CO_2RR compared to GC.

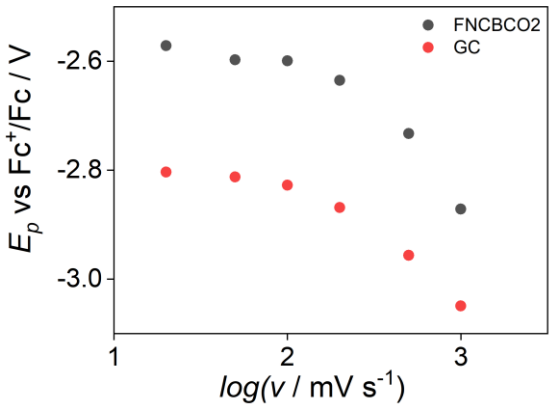

Figure 3.5 Peak potential for the reduction of carbon dioxide at different scan rates on FNCBCO2 electrodes (grey circles) and GC electrodes (red circles). All measures are made in 0.1M $TEABF_4$ in dry acetonitrile with 0.1M of CO_2.

Further experiments conflict with the first set (**Figure 3.6**). The analysis made between GC and FNCBCO2 shows both are affected by errors, the variations in the measures of FNCBCO2 are conductible to the difference in the deposit, as mentioned above. Completely different is the set of data for the GC

electrode (**Figure 3.16**), the variations between the two sets are very large compared to the ones of the FNCBCO2.

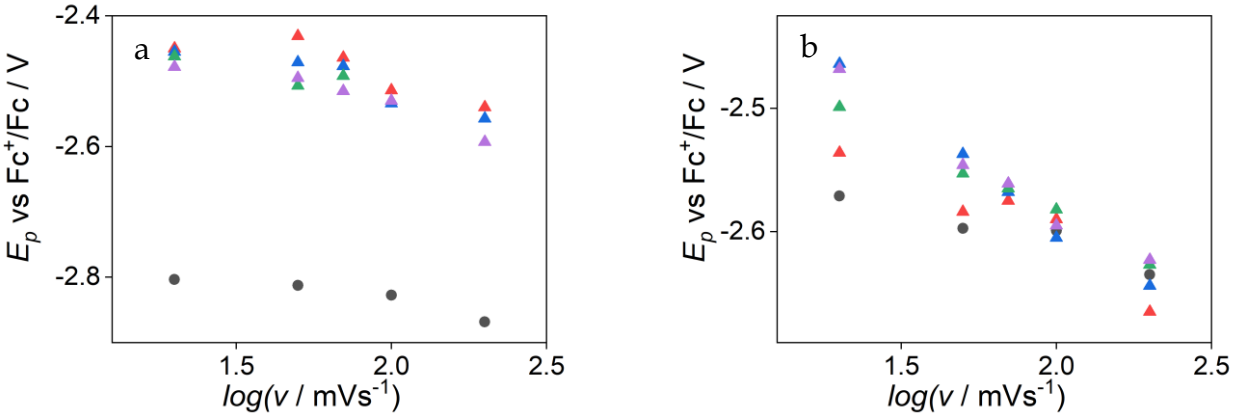

Figure 3.6 Comparison between the reliability of the GC (a) and FNCBCO2 (b). The CV were recorded in CH_3CN 0.1M $TEABF_4$ with 0.1M of CO_2. The grey circles are the data shown in **Figure 3.5**, while the triangles are repeated measures with a cleaned GC in (a) and a new deposit in (b)

This glassy carbon behaviour does not reflect the inertness that it was expected to have. An explanation of this anomaly was found comparing the cyclovoltammetry recorded with the work of Jacques Simonet[49] about the grafting of glassy carbon electrodes. As already discovered by Simonet, the glassy carbon, more in general the graphite, cannot be considered an inert surface. Below a potential threshold, Simonet sets this value at E < -1.7 V vs Ag/AgCl, the GC is negatively polarized and it starts to behave like a nucleophilic surface. The polarization does not affect only the interface of the electrode but also the inner layers, causing insertion of the ammonium salt in the material, more specifically heavily in the highly oriented pyrolytic graphite (HOPG) crystal sites present. The insertion forms "graphite salt" [C_n^- TAA^+] (TAA= tetra alkyl ammonium), where n represents the carbon in the crystal site. The insertion of the ammonium, from all points of view, is a grafting of the surface causing its modification and the change of the reactivity. Therefore, the "graphite salts" could be considered both as reducing agents and poly-nucleophilic material. The behaviour just described is the key to understanding the voltammograms in **Figure 3.**, the carbon dioxide is reduced to, $CO_2^{\bullet-}$, with the [C_n^- TAA^+], the nucleophilic salt attack the electrophilic carbon on the radical anion, leading to a carboxylation of the carbon surface. The functionalization leads to a progressive modification of the peak for the CO_2 reduction with the reduction peak decreasing in intensity and moving versus more negative potential values resembling the typical behaviour of a passivating process (**Figure 3.a**). This kind of functionalization is not irreversible, in the same work, Simonet found that in anodic range the

carboxylic group is detached by the surface and the reactivity of the GC is repristinated.

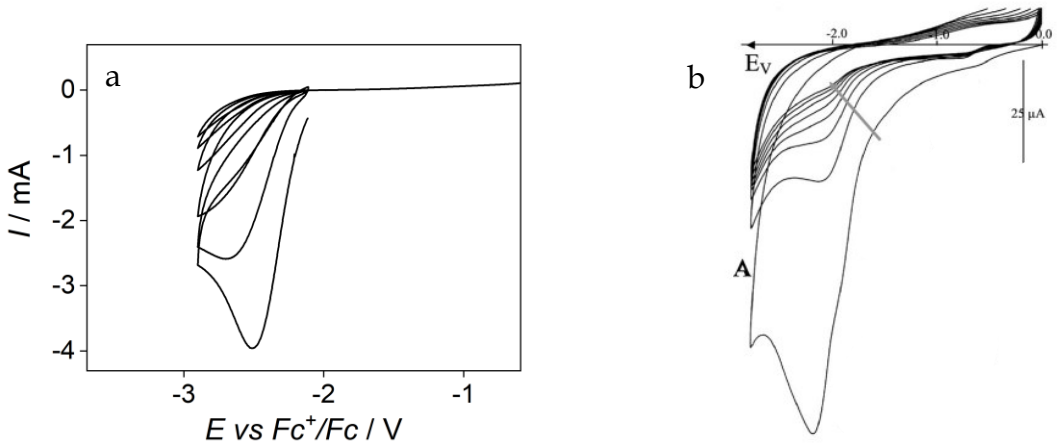

Figure 3. Comparison between the voltammetric behaviour of GC in the CO2RR recorded in this thesis project (a) and with correspondent behaviour observed by Simonet (b).

The anodic oxidation reaction on the GC passivated electrode occurs in a similar way to a non-Kolbe decarboxylation reaction where an alkylcarboxylate compound undergoes a two-electron scission of carbon-carboxylate bond with the evolution of CO_2. The decarboxylation reaction should give an anodic peak of desorption, a more symmetric one compared to a classic peak due to an electron transfer. The recorded voltammetries show an anodic peak confirming the behaviour described by Simonet. (**Figure 3.7**).

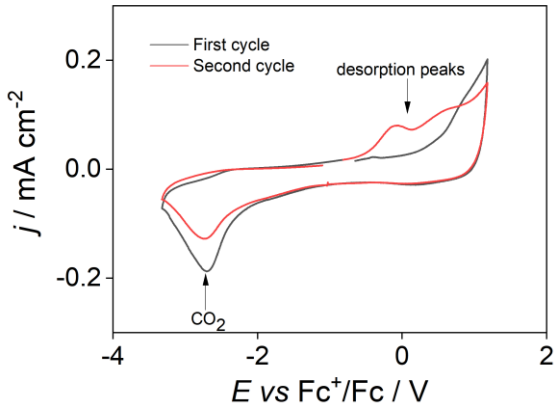

Figure 3.7 CV of the "poisoning" of the electrolyte and the desorption peaks of the electrolyte and CO_2. The CV was recorded made in CH_3CN 0.1M $TEABF_4$ with 0.1M of CO_2.

To summarize, the abnormal behaviour showed by the GC is due to a modification of the surface during the measurements; such modifications are difficult to reproduce and they were somewhat different all the time, hampering the quality of the CV response on GC.

3.2.1 Electrolysis with CO2

A further effort to understand the real capacity of the catalysts to be or not to be active in the CO_2 reduction reaction was made by means of electrolysis measurements on electrodes of large surface area prepared according to the procedures in **Chapter 2**. An electrolysis experiment with the FNCBCO2 was performed to see which products are favoured between those possible in anhydrous solvent: CO, carbonate or oxalate. The electrolysis was done in dry acetonitrile with 0.2 M of $TEABF_4$ and CO_2 saturated. The counter electrode was a platinum gauze in a separate compartment. The potential applied was -2.55 V vs Fc^+/Fc.

CO, carbonate or oxalate are the expected products from the mechanism exposed in **Figure 1.3**. According to literature findings it seems that both mechanisms are equally probable and the preference for a mechanism over the other is extremely dependent on the solvent and cathode material.

The electrolysis products were analysed qualitatively by gas-chromatography to search CO and by IR to see the formation of oxalate and carbonate. Standard solutions of oxalate and carbonate were prepared in a solution 0.1 M $TEABF_4$ in acetonitrile. The carbonate is insoluble in such conditions; therefore the formation of precipitate is expected. The IR spectrum of the solution of oxalate shows two peaks at 1645 and 1677 cm^{-1} (**Figure 3.8**).

The faradic efficiencies (F.E.), from the electrolysis are reported in **Table3.3**. For FNCBCO2 the F.E. achieved after 7 hours was 51.9%, while for the carbon paper 50%. It appears that there is no difference between the two adopted electrode: the sole carbon paper and the catalyst loaded on the carbon paper. The presence of the CO and the absence of oxalate suggests that only one mechanism is present, **Fig 1.4a**.

Carbonate should be detected in two ways, by the formation of a precipitate, carbonated salt, which is insoluble in acetonitrile, or by the IR peaks of $(EtN^+)_2CO_3^{2-}$ (or HCO_3^-). The anionic carbonate generated is counterbalanced by the ammonium cation of the electrolyte. From the literature, the IR peaks of the salt should be at 1643, 1304 and 1000 cm^{-1}.[50] The IR spectra of the solution shows two peaks typical of the carbonyl stretching. In this case, the production of formic acid is excluded, because if water were present in the electrolysis batch, the evolution of hydrogen would be detected, but this was not observed.

Figure 3.9 is the spectrum resulting from subtraction between the spectra of FNCBCO2_7h, the electrolysis solution after 7 hours, and FNCBCO2_t0, the electrolysis solution at the begin. This was made to enhance the peaks of the products and eliminate peaks of the acetonitrile and supporting electrolyte.

The peaks assigned are: 1647 cm^{-1} (CO_3^{2-}), 2987 ,2931, 1388, 1359 and 1336 cm^{-1} (DMF), 2340 cm^{-1} (CO_2). The presence of DMF is due to its unavoidable leakage from septum of the reference electrode. Therefore, the final IR is compatible with the formation of CO + carbonate, while oxalate is absent.

Table 3.3 Faradic efficiency (FE) of the electrolyses performed.

	FE (%) after 7h
FNCBCO2 [a]	51.9%
CP	50%

[a] the loading on the cathode was 0.3mg cm^{-2}.

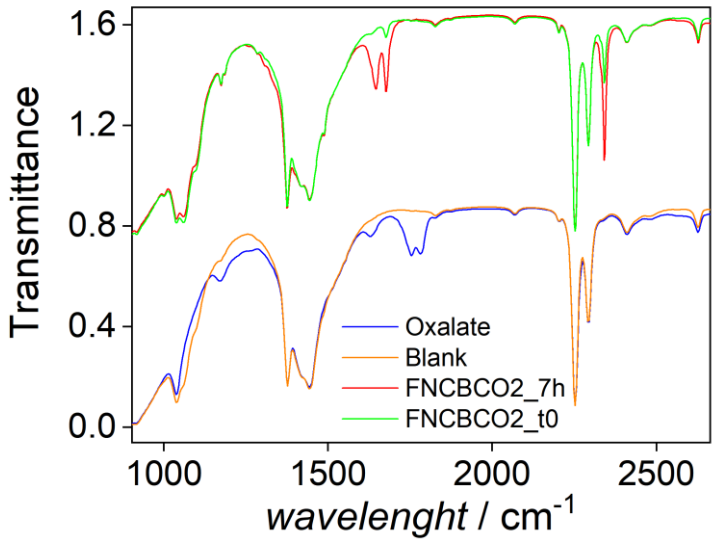

Figure 3.8 Comparison between the IR spectra of the standard solutions (orange: acetonitrile and $TEABF_4$, orange: acetonitrile, $TEABF_4$ and oxalate) and the solution of the electrolysis (green: initial solution, red: after 7h).

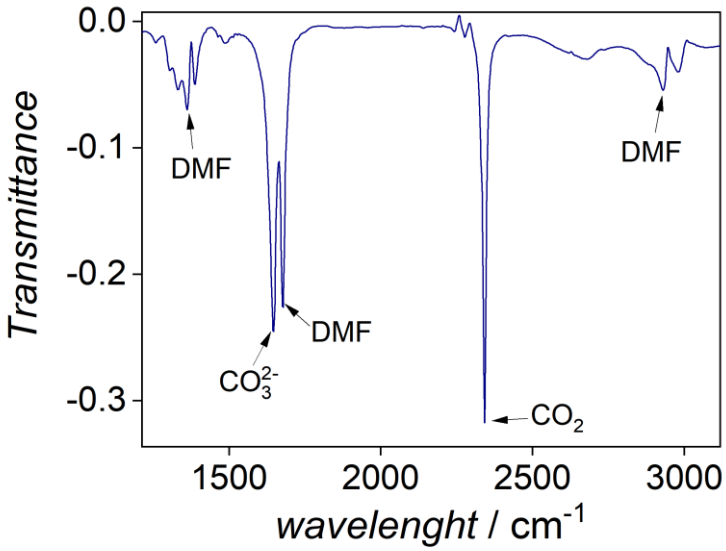

Figure 3.9 Subtraction between FNCBCO2_7h, the electrolysis solution after 7 hours, and FNCBCO2_t0 the electrolysis solution at the begin.

As partial conclusion we can assert that SASCs are not catalytically active towards the direct reduction of the CO_2 in acetonitrile, meaning that active sites commonly believed to be active in aqueous solvents, are not at all so in organic solvents, probably due to the poisoning action of the solvent itself, which coordinates axially with the metal centre, occupying the axial active site. In fact, it has been observed that the reactivity of the catalysts is quite similar or even lower than catalysts without functional FeN_4 sites or even similar to any non-functional carbonaceous material. So this would seem to pose an obstacle to using the organic environment as a platform for CO_2 reduction and reuse processes. However, the direct reduction of CO_2 is not the only way to reuse carbon dioxide, as mentioned in **1.3**. For this purpose, another strategy was adopted: the cleavage of organo-halides.

3.3 Cleavage of carbon-chloride bond

The Fe-N-C can be an interesting catalyst for the cleavage of carbon-chloride bonds since it combines the advantage of a heterogeneous catalyst with the importance of the functionalization of C-Cl bonds in a solvent, acetonitrile, largely used in organic synthesis. Few papers about the behaviour of those materials in organic media were published, so this thesis work further explores the use of Fe-N-C for the cleavage of the C-Cl bond of commodity chemicals (benzyl chloride and chloroacetonitrile).

This type of reaction aims to provide a carbon anion (R^-) from the organic halide at a low potential which can then perform a nucleophile attack on the CO_2 dissolved in solution, giving the corresponding carboxylic acid. The generation of R^- is the energetic barrier to overcome in this reaction. The activation of a carbon-chloride is extremely energy demanding, and the successive nucleophilic addition is considered fast.

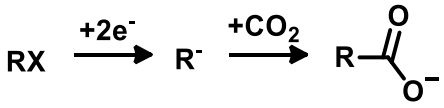

Figure 3.10 Scheme of the two consecutive reactions studied.

The substrate chosen for testing the activity of catalyst towards the C-Cl bond cleavage are benzylchloride and chloroacetonitrile; this choice was due to a simple and well-understood mechanism for the cleavage. Their carboxylic acid, respectively phenylacetic acid and cyanoacetic acid, are also relevant in industry.

Cyanoacetic acid

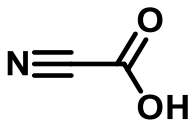

Cyanoacetic acid is a versatile intermediate in the preparation of chemicals. It is a building block for many drugs, e.g., dextromethorphan.

Phenylacetic acid

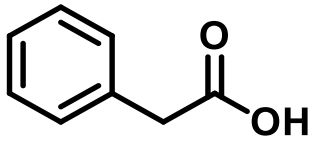

Phenylacetic acid is used in some perfumes, as it possesses a honey-like odour even in low concentrations. It is also used in penicillin G production and diclofenac production.

The bond C-Cl cleavage on glassy carbon for these two molecules was already studied by Isse *et alia.*[51] In the article is reported that the mechanism for these molecules is a concerted one, the value of α is below 0.5.

The study made by Isse *et alia* was taken as a reference, but the measures on GC electrode were repeated in order to have a confirmation on the obtained result, also considering the effect of CO_2 on the structure and reactive of the GC surface. Further, confirmation on the partial reliability of GC electrode was also explained in an article by Gennaro *et alia*.[52] Despite the GC can be considered as an inert electrode, its activity for the carbon-chloride bond cleavage is not the same for different GC electrodes. For the two considered halide containing molecules, namely chloroacetonitrile and benzylchloride, variations up to 100 mV for different GC electrodes were reported (based on the pre-treatment and preparation of the electrodes). In the article[51] it is reported that the difference in the activity is linked to the O/C ratio, where O is the oxygen adsorbed on the surface and forming carbon oxide moieties.

3.3.1 Electrochemical study of chloroacetonitrile

Cyclovoltammetries at various scan rates were recorded to study the activity of the catalyst toward the C-Cl cleavage in chloroacetonitrile. From the cyclovoltammetries recorded it is clear that FNCBCO2 is a catalytic surface for the reduction of chloroacetonitrile. The cyclovoltammetry reported in **Figure 3.11** shows a significant difference in term of peak potential between GC and FNCBCO2 (ΔE_p = 300 mV), confirming the higher activity of the last one.

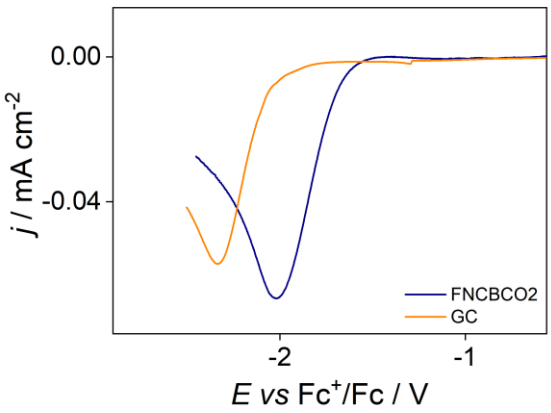

Figure 3.11 Comparison between CV recorded at 100mVs^{-1} of 5mM benzyl chloride in CH_3CN 0.1M $TEABF_4$ with GC and the catalyst. In both the CV the blank is subtracted and the return scan is omitted for clarity.

Different cyclovoltammetries at progressive scan rates were recorded, the range of scan rate chosen was 40-200mVs^{-1}. From the E_p-log$v$ plot, the value of α is calculated for the GC and the FNCBCO2 and compared with those reported in the literature.[51] The value of α was calculated to confirm that the mechanism of the cleavage is concerted, corroborating that the mechanism is independent of the material of the cathode.

Table 3.4 Values of α reported from literature and from the data collected. Calculated from $dE_p/d\log=-1.15RT/\alpha F$.

	Isse *et alia* [51]	GC	FNCBCO2
α	0.32 [a]	0.31	0.31

[a] on GC electrode

Bulk electrolysis of chloroacetonitrile was performed on GC and FNCBCO2 electrode for studying the product distribution. Since the acetonitrile was the solvent used in electrolysis only the cyanoacetic acid was followed by HPLC-UV analysis. Unfortunately, the column was too polar and even with a different ratio of acetonitrile and water it was not possible to separate the molecules; both reagent and products were eluted with the head of the solvent, thus preventing analysis of the product.

Therefore, a more polar organ halide was chosen to study the reactivity towards the C-Cl cleavage.

3.3.2 Electrochemical study on benzyl chloride

The electrochemical behaviour of the benzyl chloride was studied in the same way as the chloroacetonitrile. From the cyclovoltammetries recorded it is clear that the presence of the catalyst anticipates the peak potential, meaning that the catalyst has greater activity than the GC. The peak potential for the reduction of benzyl chloride is anticipated by over 0.3 V on FNCBCO2 (**Figure 3.12**).

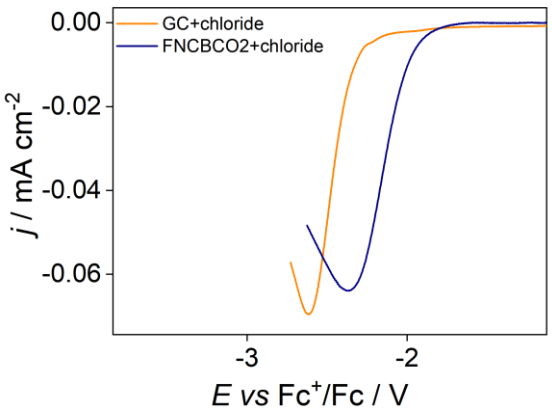

Figure 3.12 Comparison between CV recorded at 100mVs^{-1} of 5 mM benzyl chloride in CH_3CN 0.1 M $TEABF_4$ with GC and the catalyst. In both the CV the blank is subtracted, and the return scan is omitted for clarity.

Figure 3.11 Comparison between CV recorded at 100mVs-1 of 5mM benzyl chloride in CH3CN 0.1M TEABF4 with GC and the catalyst. In both the CV the blank is subtracted and the return scan is omitted for clarity.**Figure 3.12** shows that the FNCBCO2 is active also for the reduction of this organic halide, confirming the activity towards the DET of the carbon chloride bond. The

reduction peak of the benzyl chloride on the glassy carbon is at -2.61V vs Fc^+/Fc while with FNCBCO2 the potential is lowered to -2.28 V vs Fc^+/Fc

Table 3.5 Values of α reported from literature and from the data collected. Calculated from $dE_p/dlog=-1.15RT/\alpha F$.

	Isse *et alia* [51]	**GC**	**FNCBCO2**
α	0.32 [a]	0.31	0.30

[a] on GC electrode

The value of α calculated is comparable to the one reported in the article. From **Figure 3.12** shows that the FNCBCO2 is active also for the reduction of this organic halide, confirming the activity towards the DET of the carbon chloride bond. The reduction peak of the benzyl chloride on the glassy carbon is at -2.61V vs Fc+/Fc while with FNCBCO2 the potential is lowered to -2.28 V vs Fc+/Fc

Table 3.5 the mechanism is concerted on both GC and FNCBCO2. The small variations of the value of α are due to several factors, such as the carbon oxide sites or the morphology of the surface.

The graphs below, **Figure 3.13**, represent two sets of data where it is possible to see the large variations of the reduction peak potential of benzyl chloride on GC, as reported in the literature. Conversely, the catalyst seems to have a higher degree of reproducibility at FNCBCO2. This suggests that the surface of the catalyst is hardly affected by the reduction of CO_2 or other compounds happening at such negative applied potentials while the CV curve is recorded. This behaviour is also an indication of the reproducibility of the film formation for FNCBCO2. Since the bond breaking of an organic halide is highly dependent on the O/C ratio, as evident for GC surface, the reproducible behaviour of the laboratory catalyst indicates that FNCBCO2 is prepared consistently with the same surface composition.

From those data is clear that the presence of nitrogen and iron improve the reproducibility and the activity of the electrode surface towards C-Cl reduction, compared to the GC where only O sites are present. The GC surface is both less active and overall less reproducible towards the reduction of C-Cl bonds. (Note that despite the poor reproducibility of the measurements on GC, this surface is always less active that FNCBCO2.)

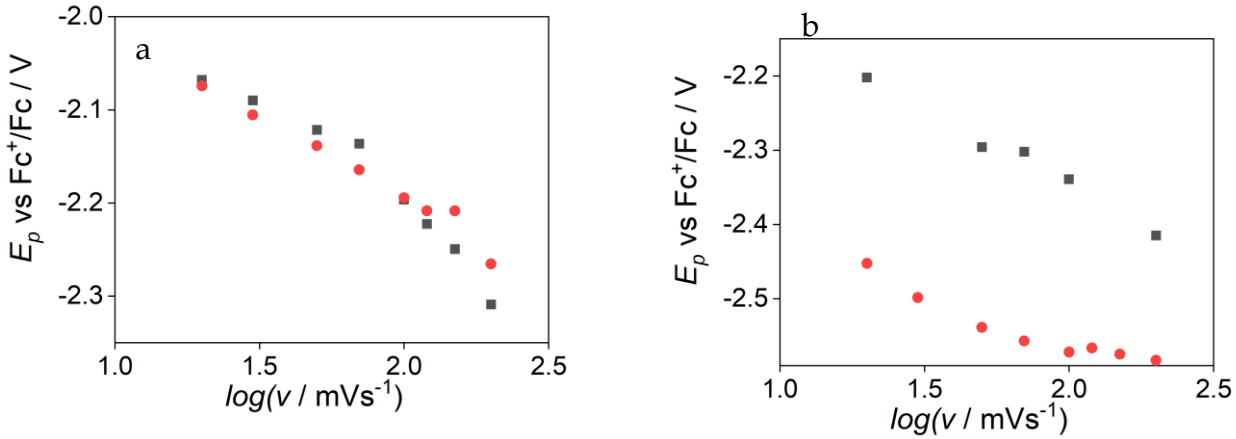

Figure 3.13 Peak potential for the reduction of benzyl chloride at different scan rates on two different FNCBCO2 electrodes (a) and two GC electrodes (b). All measures are made in 0.1M $TEABF_4$ in dry acetonitrile with 5mM of benzyl chloride.

To test the hypothesis of some heteroatoms (Fe/N) being the central catalytic site for the carbon halide bond cleavage, cyclovoltammetries at progressive scan rate were performed. The tests were done on FNCBCO2 and on a similar catalyst prepared without the metal centre (NOFe), where only N sites are present. The latter catalyst should serve as a reference to understand if there is a role of metal centre or if the main role is played by nitrogen functionalities. It is worth to mention that besides FeNx sites, FNCBCO2 also possesses nitrogen functionalities as those present in NOFe (see **Chapter 2** for details).

If we look at E_p as a descriptor of the activity towards the C-Cl bond cleavage, NOFe had similar or slightly higher catalytic activity than FNCBCO2; this suggested that the N sites are responsible for the observed catalysis, while the Fe centre did not play a significant role. This result is in partial agreement with the observations of Gan *et alia*[34], who studied the electrochemical dechlorination of 1,2-dichloroethane. They indicated that both FeN_4 sites and N sites are the dominant ones for the observed catalytic activity, but in this case it appears that FeN4 are silent in term of activity, possibly because of similar considerations already made for the reduction of CO_2

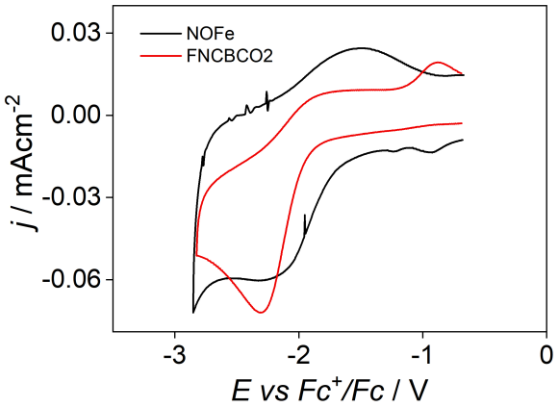

Figure 3.14 Cyclic voltammetry of 5 mM of benzyl chloride recorded at 100mV s^{-1} on the catalytic electrode with the iron centre (FNCBCO2) and the one without iron centre (NOFe). Both were recorded in 0.1M $TEABF_4$ in dry acetonitrile.

The role of nitrogen and iron was further investigated by recording cyclic voltammograms on a series of SASCs (FNCBCO2, PAJ and CNRS, whose properties are listed in **Table 3.2**) differing for the number of nitrogen functionalities and FeN_x sites.

Table 3.2

	N 1s	Imine	Pyridinic	NxFe	Pyrrolic	Graphitic	N-O
PAJ	2.3	14.4	11.6	7.1	39.4	22.1	5.4
CNRS	2.15	18.6	21.6	15.8	25.9	16.2	19
$FNCBCO_2$	0.59	19.8	27.2	17.3	30.3	5.4	0

Figure 3.15 reports CV of benzyl chloride on the three catalytic electrodes. At first glance the different CVs differs for the capacitive current (background current), which is due to the high electrochemical surface area offered by the homemade catalysts with respect to flat GC. From the CV reported in it is possible to establish an order of activity: PAJ as the major activity, CNRS and FNCBCO2 have similar activity, while GC is the least active electrode. The reduction peak potential correlates well with the amount of pyrrolic N sites. PAJ has the highest activity and the highest percentual of pyrrolic sites (39.4%) while the CNRS and the FNCBCO2 have a similar percentual of pyrrolic sites (respectively 25.9% and 30.3%). With no pyrrolic sites, GC has no catalytic activity. From these data pyrrolic N seems a good candidate as a site promoting the C-Cl cleavage in acetonitrile.

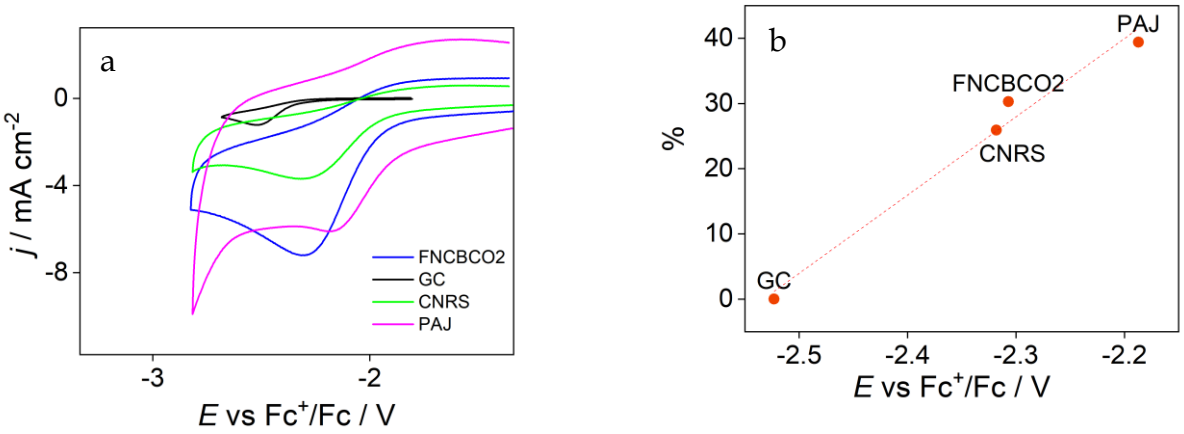

Figure 3.15 (a) Cyclic voltammetry of 5 mM benzyl chloride on the different electrodes as listed in the legend. All the measures are made in the same conditions: 0.1M $TEABF_4$ in dry acetonitrile with 5mM of benzyl chloride at 100mV s^{-1}. The GC cyclovoltammetry reported in the graph is the most reproducible one. (b) The plot of the E_p vs the percentage of pyrrolic N on total nitrogen.

Isolating the contribution of a certain site to overall catalytic activity is quite challenging. One way to do it is to selectively poison the active centre. For example, in aqueous media FeN_x could be poisoned with cyanide or thiocyanide showing a lowering in activity toward the oxygen reduction, meaning that those sites have a central role of activity. The same principle is applied for the determination of site density with NO_2^- as previously described. In this system, also the protonation of N functionalities can be used as a strategy for deactivating the N functional groups and so to investigate their role in the catalytic process. Therefore, we investigate the possible role of a proton source in the electrocatalytic process.

Cyclic voltammetry in acetonitrile at different scan rates was carried out with the addition of 2 mM of acetic acid, as a proton donor. The article of Muhammed et alia[53] showed that by changing the pH of an aqueous solution towards acidic values the activity of a SASC containing FeN_4 and N pyrrolic sites changes. This is due to the protonation of nitrogen-containing groups, that involves a lower activity in acidic solution than in basic or neutral solution. The strategy was here applied in organic media, adding acetic acid to the acetonitrile solution.

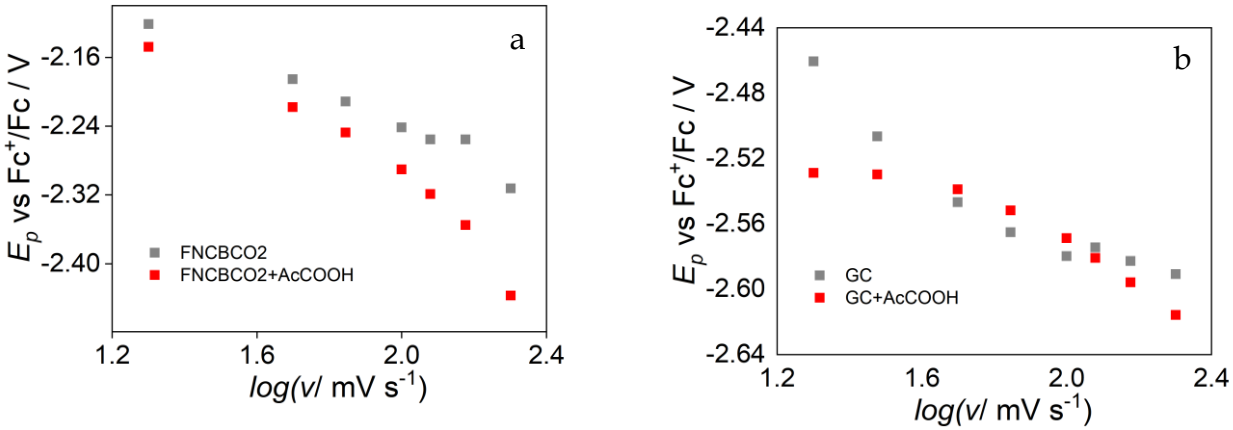

Figure 3.16 (a) Comparison between the measures on FNCBCO2 without (grey) and with 2mM of acetic acid (red). (b) Comparison between the measures on GC without (grey) and with 2mM of acetic acid (red).

The data reported in the **Figure 3.16** show that after adding the proton donor, namely acetic acid, the peak potential of the SASC changes of several mV versus more negative potential at all the investigated scan rate, the effect being more pronounced at higher scan rate. This can be further evidence that N-functionalities are the real active sites and that protonation can selectively block their activity. Conversely, on GC the effect is not plain and actually the E_p variation seem to be affected more by the variability of the measure than by the presence of a proton source. In any case, measures at GC seems to be not affected by the presence of protons.

3.3.3 Electrolysis of benzyl chloride

Potentiostatic electrolyses were performed at three different potentials selected according to peak profile recorded during cyclic voltammetry (**Figure 3.18**). This was made to see if changing the potential applied could change the selectivity between the two possible products, phenylacetic acid and toluene, taking for granted that the dimerization process is not favoured for chlorides as it is for bromides.

The phenylacetic acid is produced by the coupling of the benzylic anion and the CO_2 in solution, while the toluene is the hydrogenated product; the proton can come from residual water in the acetonitrile or by the acetonitrile itself, the pK_a of the toluene is 41 while the pK_a of the acetonitrile is 25 (**Figure 3.17**).

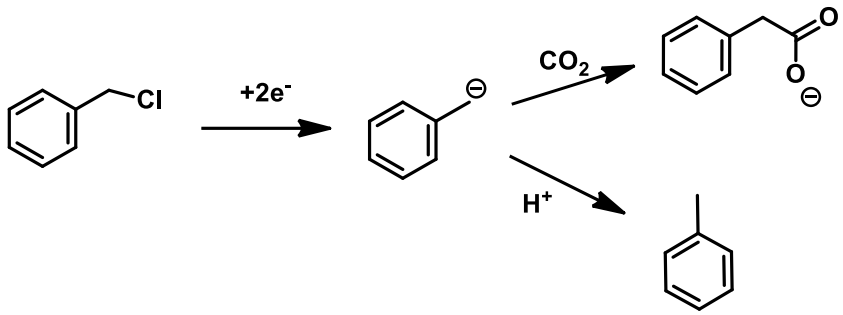

Figure 3.17 Reaction studied in electrolysis with the possible products.

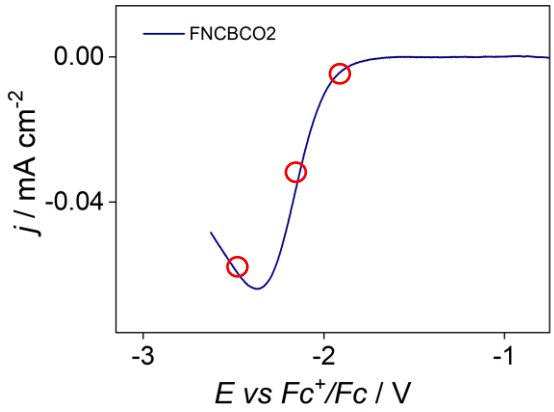

Figure 3.18 CV of 5mM of benzyl chloride at 100mV s^{-1} in 0.1M $TEABF_4$ in dry acetonitrile, the red circles indicate at which potential the electrolysis is performed.

The expected distribution of the products should show a high faradic efficiency for the generation of phenylacetic acid. Toluene should be produced with low efficiency due to the low proton availability. Decreasing the potential (towards more negative values), the faradic efficiency towards the toluene should increase, indeed in literature the hydrogenated product is favoured at more negative potentials[54].

For the electrolysis experiment, a carbon paper functionalised with FNCBCO2 was used as a cathode. For comparison, an unmodified carbon paper electrode is used as a non-catalytic cathode for the electrolysis, in the same way as GC was used in CVs†. The pristine carbon paper acts also as a blank to see if the support for the catalyst has an influence. The working electrode used was 1.5cm x 1cm with a deposit density of 0.3mg cm^{-2} in a solution of 0.2M $TEABF_4$ dry acetonitrile CO_2 saturated with 10mM of benzyl chloride. The counter electrode was a platinum gauze in a separated compartment.

The potentials chosen for the electrolysis were three:

† Glassy carbon and carbon paper are different materials, in particular on the ratio of O/C sites. A somewhat different reactivity is expected between these two materials, but carbon paper was chosen because there are not reliable and fast methods to deposit the catalyst on glassy carbon.

- The start of the reduction wave (-1.88 V vs Fc^+/Fc): at this potential, the consumption of the benzyl chloride should be the slower out of the three; the reaction should be limited by the rate of the electron transfer;
- The second potential used is at half of the wave (-2.07 V vs Fc^+/Fc);
- The third potential is after the peak (-2.40 V vs Fc^+/Fc), at this potential the rate-determining step is the mass transfer and no longer the electron transfer.

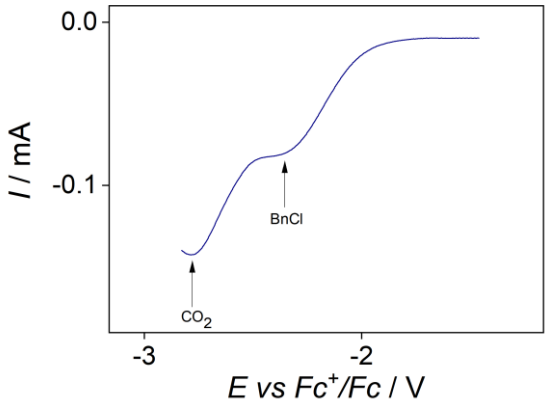

Figure 3.19 CV of the 5 mM of benzyl chloride (BnCl) recorded at 100 mV s^{-1} in a CO_2-saturated solution of dry acetonitrile with 0.1 M $TEABF_4$.

Figure 3.19 shows the cyclic voltammetry of benzyl chloride in a solution saturated in CO_2. The two reduction peaks are sufficiently separated to allow a selective reduction of benzyl chloride (E_p = -2.07 V vs Fc^+/Fc), avoiding the reduction of CO_2 (E_p = -2.70 vs Fc^+/Fc), that would decrease the faradaic efficiency. However at potentials more negative than the reduction peak for the benzyl chloride it is expected that also CO_2 starts to be reduced (the peak of the CO_2 is at -2.70 V vs Fc^+/Fc, so at -2.10 V vs Fc^+/Fc starts the onset of its reduction wave).

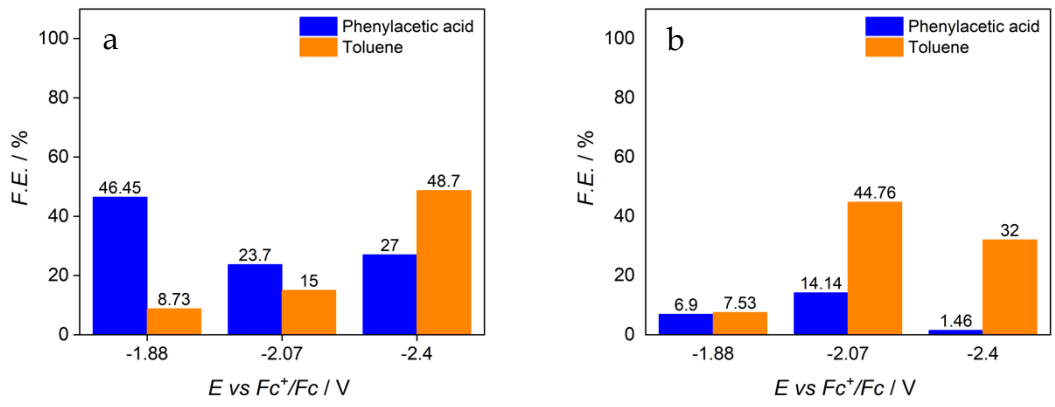

Figure 3.20. Faradic efficiency of the products obtained after 4 h of electrolysis on (a) pristine carbon paper and (b) FNCBCO2.

Figure 3.20a shows the faradic efficiency (F.E.) for the electrolysis performed with carbon paper. The F.E for toluene increases at more negative potentials, while that for phenylacetic acid increases at the most positive applied potential. Both these observations agree with literature data.[54]

Figure 3.20b shows the faradic efficiency (F.E.) for the electrolysis performed with the FNCBCO2. The F.E. is higher for toluene than for phenylacetic acid at all tested potentials. The overall F.E. shows a maximum at -2.07V vs Fc^+/Fc. Phenylacetic acid is the minority product and it is barely produced at the most negative potential.

The product yields (product concentration divided by initial benzyl chloride concentration) display a clearer picture. At more negative potentials, the yield of toluene increases for both carbon paper (**Figure 3.21a**) and FNCBCO2 (**Figure 3.21b**). The yield for the phenylacetic acid is less affected by the applied potential. For the catalyst the yield at -2.07 V vs Fc^+/Fc was the highest; the yield was very low at -1.88 V and -2.4 V vs Fc^+/Fc.

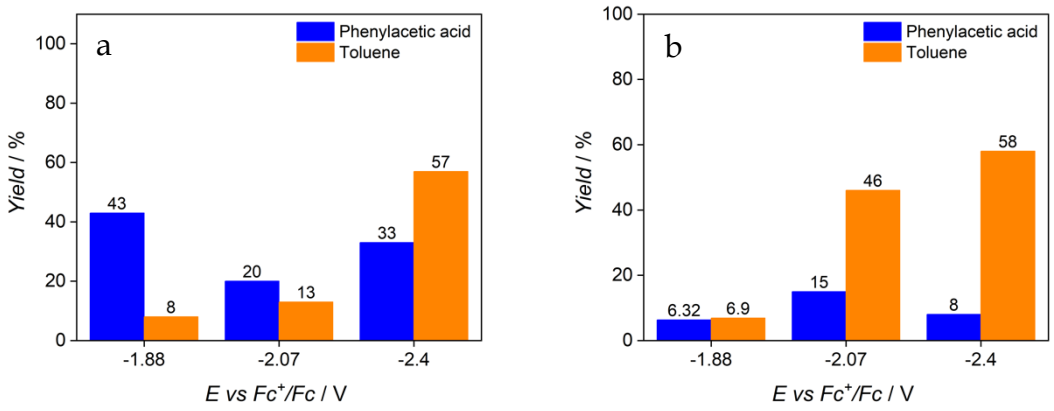

Figure 3.21. Yields of the products obtained after 4 h of electrolysis on (a) pristine carbon paper and (b) FNCBCO2.

The product distribution was followed during the entire electrolysis by sampling the solution multiple times. The determination of the products was again carried out by means of an HPLC-UV setup.

Figure 3.22a, b, c shows the product distribution over time for the electrolysis of benzyl chloride on carbon paper. The benzyl chloride was consumed faster with more negative applied potentials. The production of both toluene and phenylacetic acid increased smoothly with conversion.

Figure 3.22d, e, f shows the product distribution over time for the electrolysis of benzyl chloride on FNCBCO2. The consumption of benzyl chloride was again faster when a more negative potential was applied. At the same applied potential, the consumption of benzyl chloride was faster on FNCBCO2 than on the base carbon paper. This is in line with the catalytic effect of the

deposited FeN_x layer. The formation of toluene again increased smoothly with time. Surprising, on FNCBCO2 the production of phenylacetic acid reached a maximum and then started to decrease, which did not happen with the carbon paper only. The trend of phenylacetic acid concentration resembled that of an intermediate: at the beginning the rate of production is high and after reaching a maximum production starts to be consumed faster. This behaviour is enhanced when the electrolysis was done at –2.40V vs Fc^+/Fc, when the maximum concentration of phenylacetic acid was reached in less time, **Figure 3.22f**. From the data collected in **Figure 3.22** it is clear that the unexpected reactivity towards the benzyl chloride—and especially the phenylacetic acid reaching a maximum concentration—must be attributed only to the FNCBCO2 and not to the support.

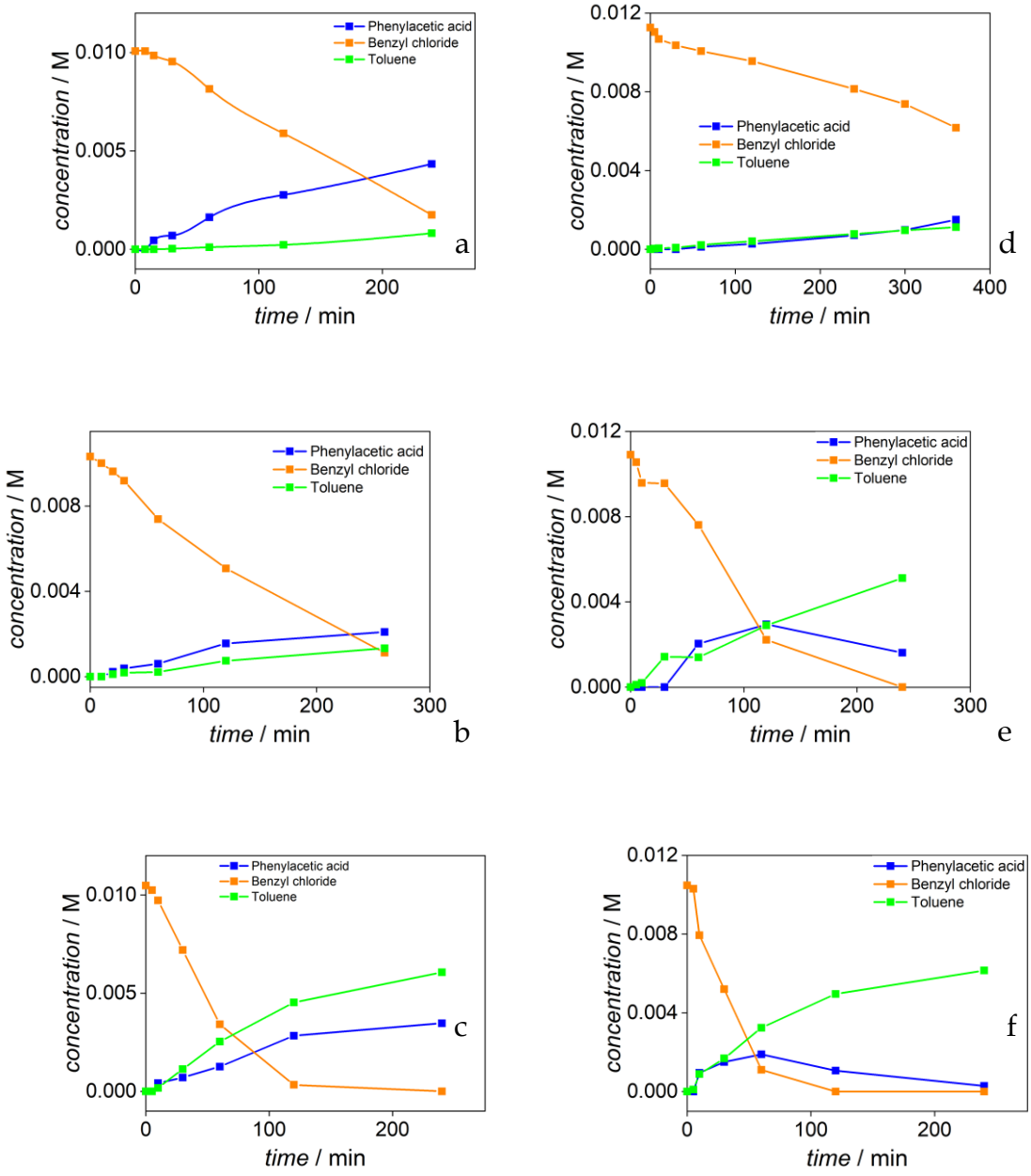

Figure 3.22 (a) Electrolysis of 10mM benzyl chloride with FNCBCO2 in 0.1M $TEABF_4$ in dry acetonitrile saturated with CO_2, the potential applied was -1.88 V vs Fc^+/Fc . (b) Electrolysis of 10mM benzyl chloride with FNCBCO2 in 0.1M $TEABF_4$ in dry acetonitrile saturated with CO_2, the potential applied was -2.07 V vs Fc^+/Fc . (c) Electrolysis of 10mM benzyl chloride with FNCBCO2 in 0.1M $TEABF_4$ in dry acetonitrile saturated with CO_2, the potential applied was -2.4 V vs Fc^+/Fc. (d) Electrolysis of 10mM benzyl chloride with carbon paper in 0.1M $TEABF_4$ in dry acetonitrile saturated with CO_2, the potential applied was -1.88 V vs Fc^+/Fc. (e) Electrolysis of 10mM benzyl chloride with carbon paper in 0.1M $TEABF_4$ in dry acetonitrile saturated with CO_2, the potential applied was -2.07 V vs Fc^+/Fc. (f) Electrolysis of 10mM benzyl chloride with carbon paper in 0.1M $TEABF_4$ in dry acetonitrile saturated with CO_2, the potential applied was -2.4 V vs Fc^+/Fc.

In the literature there are no reports about a further electrochemical reduction of the phenylacetic acid. Few papers were published about the electrochemical behaviour of carboxylic acids. One paper[55], in particular, show that aromatic carboxylic acids can be electrochemically reduced to the respective aldehyde and alcohol. In the presence of an organ halide, even the esterification can occur. It was also reported that the reduction can also proceed further and break the aromaticity of the phenyl ring.

To test if the phenylic acid can be reduced by the cathode, electrolysis of the sole phenylacetic acid was performed. Phenylacetic acid was reduced on FNCBCO2 and without the presence of CO_2. After 4h of electrolysis at -2.4 V vs Fc^+/Fc the phenylacetic acid was nearly completely consumed (**Figure 3.23a**). The result of the electrolysis of phenylacetic acid supports the results previously obtained during the electrolysis of benzyl chloride. Phenylacetic acid can be quickly reduced at the applied potential.

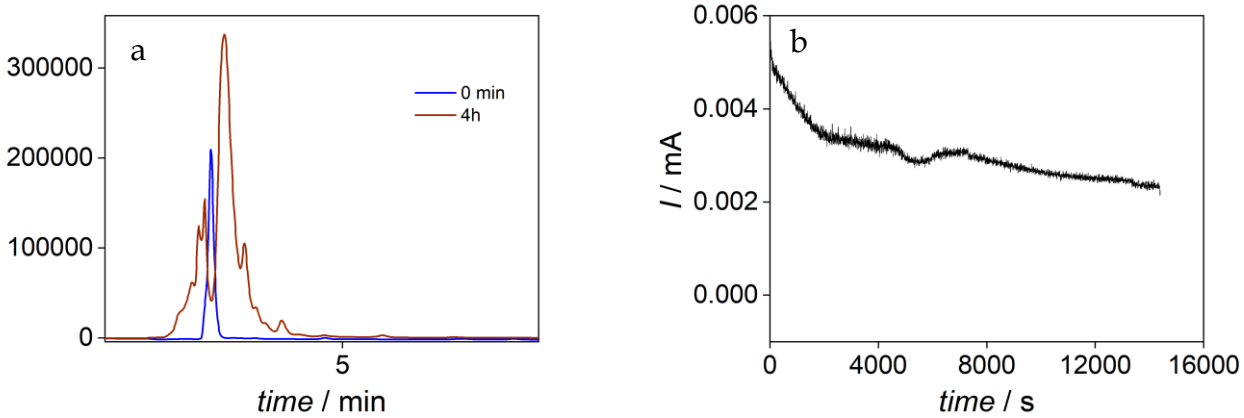

Figure 3.23 (a) HPLC chromatograms of the electrolysis products of 10mM of phenylacetic acid, after 5 minutes no further peaks were detected. (b) Chronoamperometry recorded during the electrolysis.

It was not possible to clearly identify the products of the electrolysis of the phenylacetic acid. Multiple peaks appeared at a retention time similar to that of phenyl acetic acid. According to the literature the alcohol and aldehyde should be the products. Therefore, standard solutions of phenyl ethanol and

phenylacetaldehyde were made. The phenyl acetaldehyde has a retention time similar to the highest peak, but it was not identified unambiguously, because it was not possible to improve the resolution of the HPLC separation. Different ratios of eluents (acetonitrile and water) were tested but none of them provided a good enough separation to unambiguously assign the peaks of the products of the electrolysis. Nevertheless, different products are present in the solution and all of them are polar; their retention times are near the retention time of the phenylacetic acid.

To further investigate the electrochemical behaviour of phenylacetic acid, cyclovoltammetries at different scan rates were performed on GC and FNCBCO2. From **Figure 3.25** it is clear that the acid can be reduced on both materials. However, this peak is anticipated of almost 300 mV on the catalytic electrode. The cyclic voltammetry is composed of two peaks, where the first one is assigned to the reduction of the acidic proton. (**Figure 3.24**).

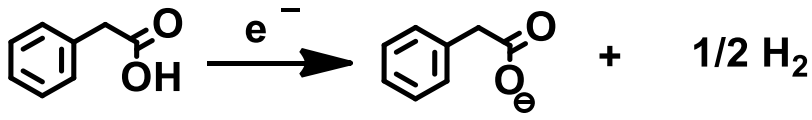

Figure 3.24 Reduction reaction of the acidic proton.

The second reduction peak at more negative potential and with a smaller peak current can be assigned to the further reduction of the phenylacetate anion even if this assignation cannot be completely unambiguous since a current intensity of the second peak is much smaller than what expected.

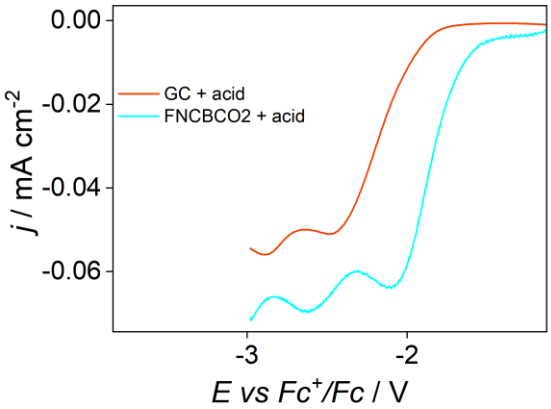

Figure 3.25 Comparison between CV recorded at 100mVs^{-1} of 5mM phenylacetic acid in CH_3CN 0.1M $TEABF_4$ with GC and the catalyst. In both the CV the blank is subtracted.

This cyclic voltammetry data helps to draw a better image of what happens during the electrolysis. In electrolysis under reductive conditions the product of coupling is not phenylacetic acid but 2-phenylacetate, the conjugate base of the acid (see mechanism in **Figure 3.26**).

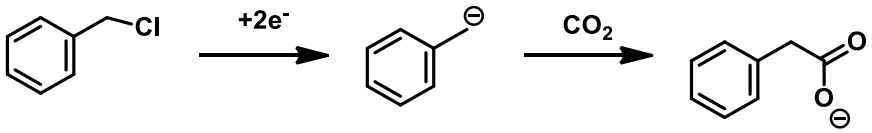

Figure 3.26 Reaction of the benzyl chloride to phenylacetate.

In **Figure 3.25** the first peak can be assigned to the reduction of the phenylacetic acid to phenyl carbonate, the reaction is described in **Figure 3.24**. The second reduction peak, as already said, is a father-son/carbonate reduction. In virtue of the fact that the electrolysis was carried out at -2.40 V vs Fc^+/Fc, the reduction process involved the second peak. Furthermore, the reduction of carbonate is catalysed by the FNCBCO2 (this becomes clear looking at the second peak potential recorded at GC with respect to FNCBCO2) that explains its consumption during the electrolysis.

Figure 3.27 shows a comparison of all CVs for the involved reagent (benzylchloride) and product/intermediate (phenylacetate). It appears that that at applied potential of -2.40 V vs Fc^+/Fc for the FNCBCO2 the benzyl chloride reduction is controlled by the mass transfer and the reduction peak of the phenylacetate is under kinetic control (we are approximately at the half peak potential of the second peak). This explains why at a more negative potential the phenylacetic acid is quickly produced and quickly consumed, so that a maximum of its concentration is observed sooner in the reaction. For the carbon paper, the benzyl chloride is under kinetic control while the reduction peak of the carbonate is too negative to give a contribution. In other words, phenyl acetate was not reduced at these potentials on carbon paper.

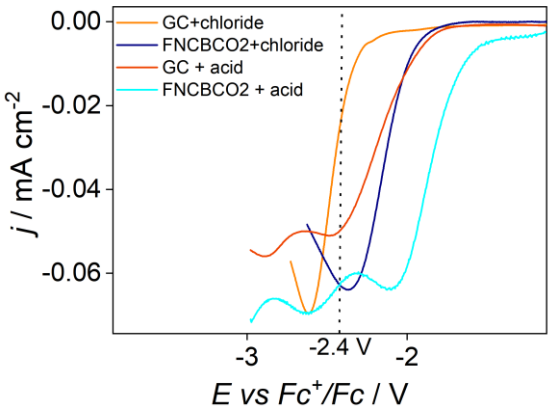

Figure 3.27 Comparison between the CV recorded in 0.1M $TEABF_4$ in acetonitrile with benzyl chlorid0(5mM) and with phenylacetic acid(5mM), the scan rate was 100mV s^{-1}.

On FNCBCO2 the reduction peak of the acid is at -2.10 V vs Fc^+/Fc while the benzyl chloride shows a peak reduction at -2.36 V vs Fc^+/Fc. From a thermodynamic point of view the reduction of the acid is strongly favoured compared to the chloride; this means that if some acid is produced (the

phenylacetate is protonated by residual water), it is quickly reduced back to acetate.

The same reasoning can be transposed to the GC (carbon paper in the case of electrolysis): the phenylacetic acid has its reduction peak at -2.48 V vs Fc^+/Fc while the benzyl chloride shows a reduction peak is at -2.61 V vs Fc^+/Fc. In the electrolysis with the carbon paper there is no evidence of an reduction of phenyl acetate because its reduction peak is too negative.

The phenylacetic acid in **Figure 3.22** behaves as an intermediate according to the following kinetic equations, where A is benzyl chloride, B phenylacetic acid, and C the reduction product(s) of phenylacetic acid.

$$A \overset{k_1}{\rightarrow} B \overset{k_2}{\rightarrow} C \qquad \textbf{Eq 3.1a}$$

$$\frac{d[B]}{dt} = k_1[A] - k_2[B] \qquad \textbf{Eq 3.1b}$$

Equation 3.1 (a) Simplification of the reduction of benzyl chloride (A) to the product of reduction of the phenylacetic acid. (b) Equation of the rate for the intermediate B. In this simplified scheme the contribution of reduction to toluene is omitted for simplicity.

When B behaves as an intermediate with the reaction profile that reaches a maximum and then goes down, initially $k_1[A]$ is bigger than $k_2[B]$ until the maximum where $k_1[A]$ is equal to $k_2[B]$; after that $k_2[B]$ becomes the predominant contributor to the equation and the concentration of B diminishes. This is what is seen during the electrolysis on the FNCBCO2.

The phenylacetic acid during the electrolysis with the carbon paper profile is different from that described above. Its concentration increases over time; therefore, in this case the contribution of $k_2[B]$ is null or very small compared to $k_1[A]$.

3.3.4 Fitting of the kinetics curves

The profiles of the reagent and products concentrations in **Figure 3.22** were modelled to extract the kinetic constants of the reactions occurring at the electrode. This allowed to confirm the proposed model (**Eq. 3.1**) from a quantitative point of view. Fittings of the kinetics were done using Predici software. The aim was to estimate the kinetic constants of the reactions.

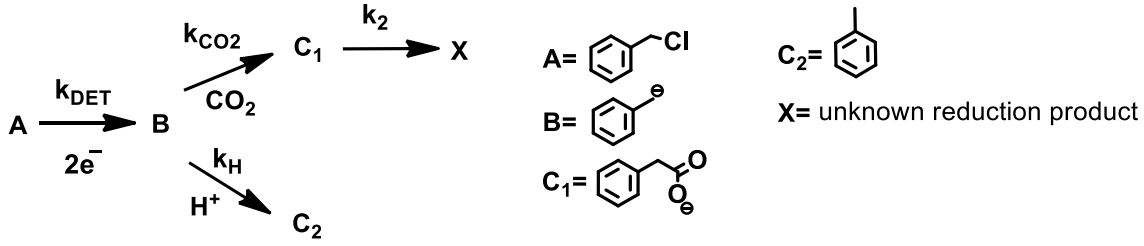

Figure 3.28 Scheme of all the reactions present in the electrolysis.

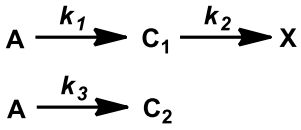

Figure 3.29 Scheme simplified.

In **Figure 3.28** all the reactions are displayed. Simulating all these reactions could be challenging, but some simplification can be made as explained in detail below. Briefly, the electrochemical reduction of benzyl chloride was modelled as a first order reaction in agreement with literature. [56] B is considered extremely active, and its reactivity is extremely fast, so it behaves as a low concentration intermediate in stationary state. Based on these assumptions, k_1 contains the contribution of the electron transfer and the contribution given by the coupling with the CO_2. k_2 is the kinetic constant of the further reduction of the carbonate. k_3 contains the contribution of the electron transfer and the contribution given by the protonation. The full derivation of the kinetic model is explained below.

3.3.4.1 Derivation of the kinetic model

First, it is necessary to write the chemical reaction and the kinetic equation for each reaction:

Chemical reaction	**Rate equation**
$RX \xrightarrow{k_{DET}} R^-$	$v_{DET} = k_{DET}[RX]$
$R^- + CO_2 \xrightarrow{k_{CO2}} RCOO^-$	$v_{CO2} = k_{CO2}[R^-][CO_2]$
$R^- + H^+ \xrightarrow{k_H} RH$	$v_H = k_H[R^-][H^+]$
$RCOO^- \xrightarrow{k_{RED}} X$	$v_{RED} = k_{RED}[RCOO^-]$

"H^+" is a proton that can be provided by adventitious water or by the solvent.

For the anion R^-, it is possible to apply the stationary state because is an extremely reactive species.

$$\frac{d[R^-]}{dt} = 0 = k_{DET}[RX] - k_{CO2}[R^-][CO_2] - k_H[R^-][H^+]$$

A further approximation can be done, [CO_2] can be collected in the kinetic constant. In fact, its concentration can be considered constant, in the solution the CO_2 is 0.3 M against a 10 mM of benzyl chloride. The same reasoning can be done for [H^+], supposing that the proton came from the solvent. After those approximations the previous equation become:

$$\frac{d[R^-]}{dt} = 0 = k_{DET}[RX] - k_{CO2}{}^{I}[R^-] - k_H{}^{I}[R^-]$$

where $k_{CO2}{}^{I}$ is equal to $k_{CO2}[CO_2]$ while $k_H{}^{I}$ is equal to $k_H[H^+]$.

Now it is possible to calculate [R^-] and to substitute it in the equation of v_{CO2} and v_H.

$$[R^-] = \frac{k_{DET}[RX]}{k_{CO2}{}^{I} + k_H{}^{I}}$$

$$v_{CO2} = k_{CO2}{}^{I} \frac{k_{DET}[RX]}{k_{CO2}{}^{I} + k_H{}^{I}}$$

$$v_H = k_H{}^{I} \frac{k_{DET}[RX]}{k_{CO2}{}^{I} + k_H{}^{I}}$$

Looking at the new equation of v_{CO2} and v_H, collecting all the constants into one allows to obtain the following final kinetic equations.

$$v_{CO2} = k_1[RX]$$

$$v_H = k_3[RX]$$

where $k_1 = k_H{}^{I} \frac{k_{DET}}{k_{CO2}{}^{I} + k_H{}^{I}}$ and $k_3 = k_H{}^{I} \frac{k_{DET}[RX]}{k_{CO2}{}^{I} + k_H{}^{I}}$. The last equations are the *pseudo*-first-order equation used to calculate the constants k_1 and k_3 and are those used in **Figure 3.29.**

The final model thus become:

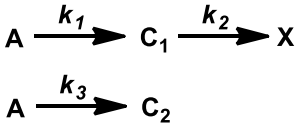

Figure 3.30 Simplified kinetic scheme.

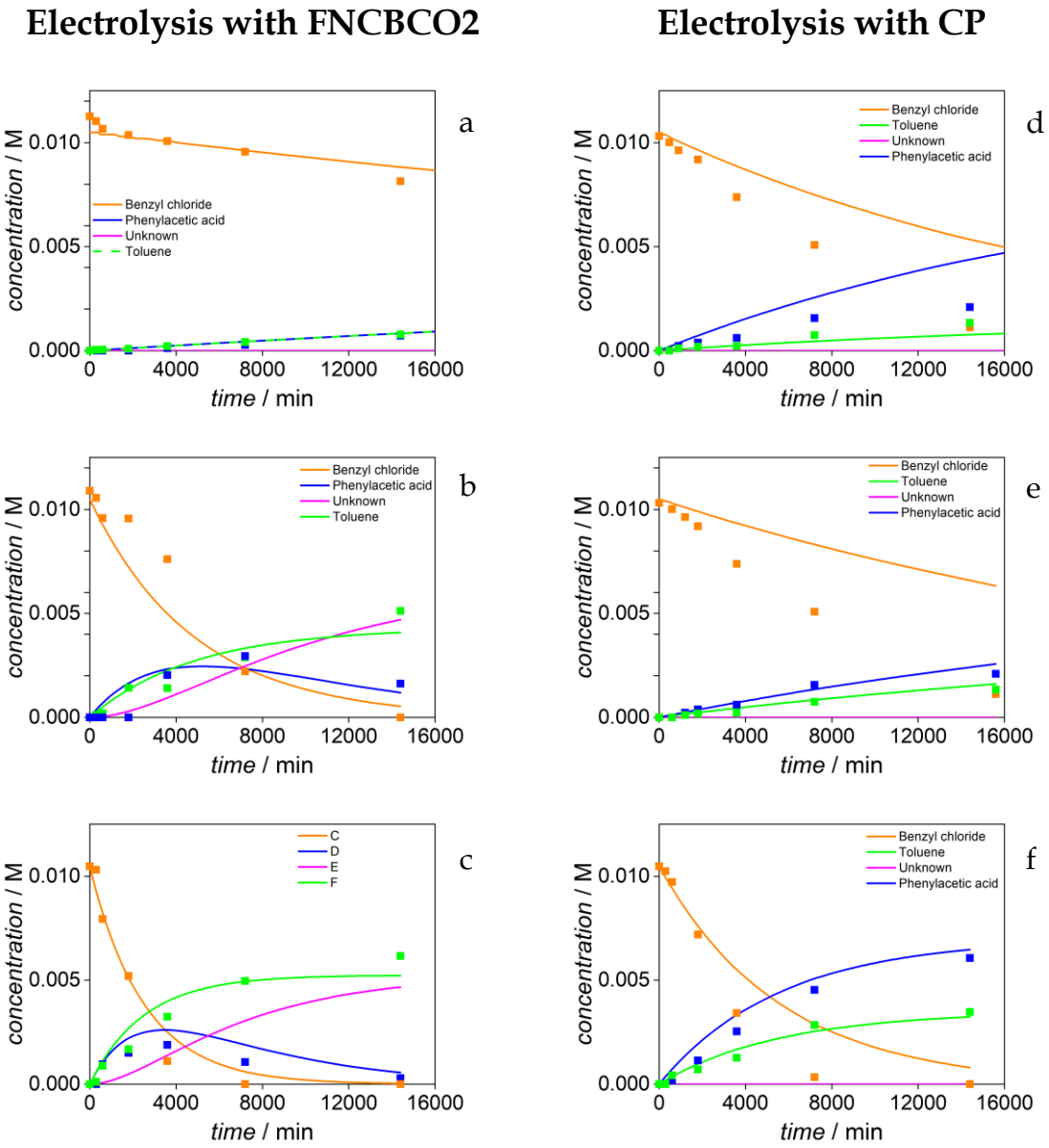

Figure 3.31 (a) Fitting of the data of the electrolysis at -1.88V vs Fc^+/Fc with FNCBCO2. (b) Fitting of the data of the electrolysis at -2.07V vs Fc^+/Fc with FNCBCO2. (c) Fitting of the data of the electrolysis at -2.40V vs Fc^+/Fc with FNCBCO2. (d) Fitting of the data of the electrolysis at -1.88V vs Fc^+/Fc with carbon paper. (e) Fitting of the data of the electrolysis at -2.07V vs Fc^+/Fc with carbon paper. (f) Fitting of the data of the electrolysis at -2.40V vs Fc^+/Fc with carbon paper.

Figure 3.31 shows the fitting of the kinetic model in **Figure 3.29** on the experimental data for the electrolysis on both the catalytic and non-catalytic electrodes. The model could provide an good fitting of the experimental data, especially the ones of the electrolysis on FNCBCO2.

Table 3.6 displays the best-fit kinetic constant for the electrocarboxylation of benzyl chloride on FNCBCO2 at the different applied potentials. The value of k_3 diminishes when the applied potential is more positive. The behaviour of k_3 is expected because moving towards more positive potential, far from the second reduction peak of the phenylacetic acid, the electronic transfer is less favoured.

The values of k_1 and k_2 are the same at all the applied potentials. This indicates that the FNCBCO2 surface has similar selectivity for both toluene and phenylacetic acid (but the latter is also continuously consumed at the electrode with rate constant k_3).

Using the data from the electrolysis with FNCBCO2 at -2.40V vs Fc^+/Fc the kinetic constants calculated are all the same, it is plausible because at that potential the rate determining step is the mass transfer, and all reactions proceed at a similar rate (**Figure 3.27**).

Table 3.6 Value of the kinetic constants calculated from the data of the electrolysis performed with FNCBCO2.

FNCBCO2	**-2.40V**	**-2.07V**	**-1.88V**
$\mathbf{k_1}$	3.0 E-04	1.2 E-04	5.2 E-06
$\mathbf{k_2}$	3.0 E-04	1.0 E-04	1.1 E-10
$\mathbf{k_3}$	3.0 E-04	1.2 E-04	5.2 E-06

The fitting of the data from the electrolysis with the carbon paper gives a quite different scenario (**Table 3.7**) The kinetic constant of the further reduction of the carbonate, k_2, is equal to zero, because the electrolysis is performed far away from the second reduction peak of the phenylacetic acid. The values of both k_1 and k_3 increase with decreasing applied potential, which is expected because the electron transfer is faster. At the potential of -2.07 V and -1.88 V vs Fc^+/Fc the fitting is particularly bad, probably the model used does not consider any parasitic reactions, which seems to give a relevant contribution.

Table 3.7 Value of the kinetic constants calculated from the data of the electrolysis performed with FNCBCO2.

CP	**-2.40V**	**-2.07V**	**-1.88V**
$\mathbf{k_1}$	6.0 E-05	1.2 E-05	5.0 E-06
$\mathbf{k_2}$	0.0	0.0	0.0
$\mathbf{k_3}$	1.2 E-04	2.0 E-05	4.0 E-05

The results obtained show that the further reduction of the phenylacetic acid plays an important role at more negative potential when the electrolysis is done with the FNCBCO2. At the most negative potential with FNCBCO2, the mass transfer is probably the rds, meaning that the kinetic constant for the further reaction of the phenylacetate is limited by the rate of mass transfer. Using the carbon paper the second reduction of the phenylacetate is absent (k_2=0), confirming the data obtained within CVs, **Figure 3.27**.

5 Conclusion

This work aimed to study FeN_x doped carbons in an aprotic solvent, towards the reduction of CO_2 and the utilization of CO_2 in electrocarboxylation reactions. Acetonitrile was the solvent of choice since its exhibit the highest reported CO_2 solubility.

From cyclovoltammetries and electrolysis it appears that the FeN_x doped carbons do not catalyse the CO_2RR in acetonitrile. The reason behind this inactivity is not clear and further studies could be done to test if the solvent has a significant contribution to the catalysis, perhaps "poisoning" the Fe sites via strong coordination. This was explained considering the stronger coordination ability of CH_3CN with respect to H_2O, which is a solvent where FeN_x doped carbons can catalysed the reduction of CO_2.

SASCs seem to be good candidates as catalysts for the carbon-halide cleavage. The DET of the C-Cl bond of benzyl chloride and chloroacetonitrile is anticipated by about 0.3 V compared to the reaction on GC. It is worth to mention that such catalytic effects were previously observed only on noble or coin metals such as Pd, Au, Cu and most of all Ag. The catalysis seems to be promoted by the pyrrolic sites as seen in **Figure 3.15**. Further experiments must be done to confirm this trend and to study the mechanism of the cleavage on the sites. It is clear that this investigation represents a proof of concept meaning that more alkyl halides must be studied to corroborates the observation collected in this thesis project. In particular those ones that go under a stepwise mechanism should have an interesting reactivity. The stepwise mechanism includes an intermediate, see **Figure 5.1**, maybe its presence can play a non-innocent role on the surface of the electrode with a probable interaction/adsorption that would justify the catalytic effect. Also, bromide and iodide could be indagated, they have a more positive reduction peak compared to the respective chloride. This would prevent to incur in side reactions taking place at more negative potentials. [57]

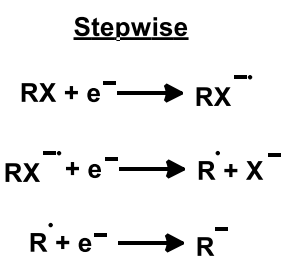

Figure 5.1 Stepwise DET.

The catalytic reduction of the phenylacetic acid was quite unexpected. Actually, the CV of phenylacetic acid shows two reduction peaks, where the identity of the second one must be investigated. In literature it is reported that not all the

organic acids have two reduction peaks, and whenever present the product of this second reduction in not identified.[58] This means that a more detailed study on the reduction of carboxylic acid can be done to improve the knowledge on this reactivity especially on nitrogen doped carbons, which appeared to open the road to a new type of reactivity.

6 Appendix

6.1 Gibbs-Marangoni effect: a brief overview

"*Look not thou upon the wine when it is red, when it giveth his colour in the cup, when it moveth itself aright*"

(Proverbs 23:31)

The Gibbs-Marangoni effect plays an important role, not only in drop-casting but in different fields, e.g., the manufacture of integrated circuits or in soaps stabilization. A weak Marangoni flow is the cause of a typical coffee ring pattern in a drop-casting deposit.

The origin of the coffee-ring pattern is caused by two factors contribution the Gibbs-Marangoni effect and capillary flow. These two phenomena cause an internal motion in the drop changing the local concentration of solute. In general, those two contributions contrast each other.

When a drop of pure liquid dries on a smooth substrate, then the base of the drop shrinks but the contact angle remains fixed. The capillary flow is caused when a drop of colloidal suspension or solution evaporates and, in contrast to the pure solvent, the drop keeps a spherical-cap shape with a constant base, in this way the height in each point of the profile decreases with time. The base is maintained constant over time thanks to the capillary flow, an outward flow that replenished the evaporated liquid at the edges of the drop with a flow of liquid from the interior (**Figure 6.1**). This flow is capable of transferring 100% of the solute to the contact line and this accounts for the strong perimeter concentration of many stains.

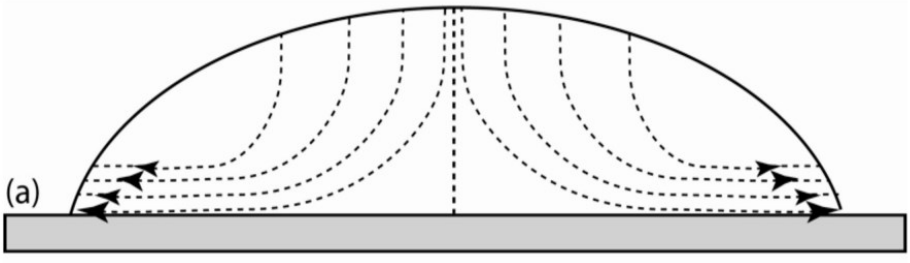

Figure 6.1 Schematic of outward capillary flow during the drying process.

The Gibbs-Marangoni effect is a circular inner motion of the particles in a drop (**Figure 6.2**), this motion is caused by a surface tension gradient which may be related to temperature variation along the free liquid surface. The liquid moves at the liquid-gas interface, from a lower surface tension point to a higher surface tension point. The non-uniform evaporation of liquid causes a

temperature gradient, and consequently a surface tension gradient along with the liquid-gas interface which drives the flow inside the liquid; this non-uniform evaporation is caused by the shape of the drop itself, the edges have a higher contact surface with the air causing a faster evaporation rate.

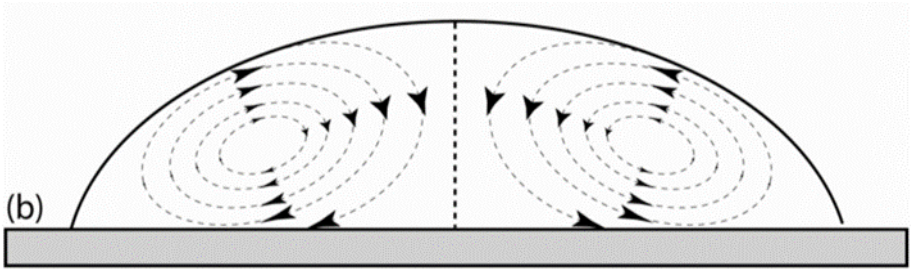

Figure 6.2 Schematic of Gibbs-Marangoni flow during the drying process.

Despite the capillary flow cannot be controlled, the Gibbs-Marangoni effect can be easily controlled by the choice of solvent or mix between different solvents, this helps to change the surface tension, or by controlling the temperature and the humidity during the evaporation time.

The ideal solution is a solvent (or a mix of solvents) with low superficial tension, the drop will be flat, and a high vapour tension, these two factors help have homogeneous and fast evaporation, the last point minimizes the formation of thermal motion inner the drop. A small drawback is present if the evaporation is too fast the deposit will be collected only in the centre of the drop, causing the reverse coffee ring effect. A chamber where the temperature and the moisture are kept constant also can minimize the formation of a coffee ring.

Figure 6.3 Drawing of the three cases, from the left: a coffee ring effect deposit, a perfectly homogeneous deposit and a reverse coffee ring deposit.

6.2 Calibration for the liquid products

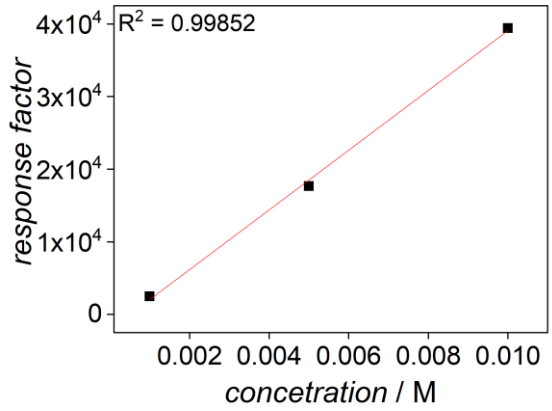

Figure 6.4 Calibration of the benzyl chloride with the HPLC. The eluent was 60:40 acetonitrile/water with a flux of 1mL/min and the detector set at 250nm. The retention time is 7.9 min.

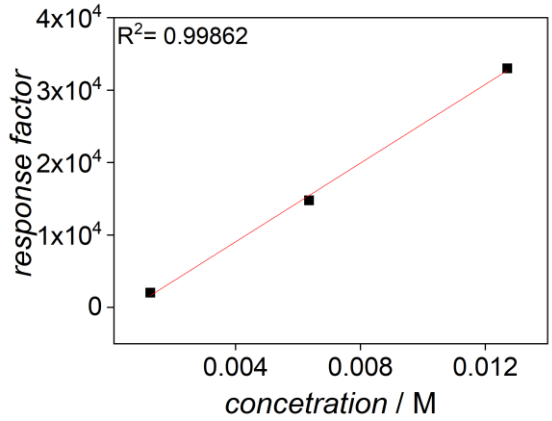

Figure 6.5 Calibration of the phenylacetic acid with the HPLC. The eluent was 60:40 acetonitrile/water 1mL/min and the detector was set at 250nm. The retention time is 3.4 min.

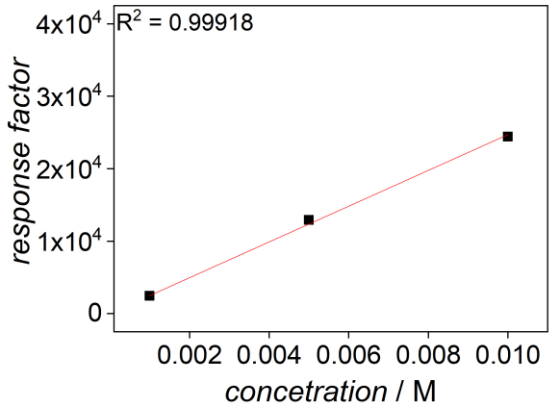

Figure 6.6 Calibration of the toluene with the HPLC. The eluent was 60:40 acetonitrile/water 1mL/min and the detector was set at 250nm. The retention time is 10 min.

7 Bibliography

(1) IPCC_AR6_WGI_SPM_final.pdf https://www.ipcc.ch/report/ar6/wg1/downloads/report/IPCC_AR6_WGI_SPM_final.pdf.

(2) Jinyue Y., Zhien Z. Carbon Capture, Utilization and Storage, Applied Energy Volume 235, 1 February 2019, Pages 1289-1299 . https://doi.org/10.1016/j.apenergy.2018.11.019

(3) https://www.ipcc.ch/site/assets/uploads/2018/03/srccs_wholereport-1.pdf

(4) *Carbon Dioxide as a Source of Carbon*; Aresta, M., Forti, G., Eds.; Springer Netherlands: Dordrecht, 1987. https://doi.org/10.1007/978-94-009-3923-3.

(5) Schneider, J.; Jia, H.; Muckerman, J. T.; Fujita, E. Thermodynamics and Kinetics of CO2, CO, and H+ Binding to the Metal Centre of CO2reductioncatalyst. *Chem Soc Rev* **2036**, *41*, 2036–2051. https://doi.org/10.1039/c1cs15278e.

(6) Allen J Bard. *Standard Potentials in Aqueous Solution*, 1st ed.; CRC Press, 1985.

(7) Ito, K.; Ikeda, I.; Yamauchi, N.; Iida, T.; Takagi, T. Electrochemical Reduction Products of Carbon Dioxide at Some Metallic Electrodes in Nonaqueous Electrolytes. *Bull Chem Soc Jpn* **1985**, *58*, 3027–3028.

(8) Ikeda, S.; Takagi, T.; Ito, K. Selective Formation of Formic Acid, Oxalic Acid, and Carbon Monoxide by Electrochemical Reduction of Carbon Dioxide. *Bull Chem Soc Jpn* **1987**, *60*, 2517–2522.

(9) Goodridge, F.; Presland, G. The Electrolytic Reduction of Carbon Dioxide and Monoxide for the Production of Carboxylic Acids. *J. Appl. Electrochem.* **1984**, *14* (6), 791–796. https://doi.org/10.1007/BF00615269.

(10) Boutin, E.; Salamé, A.; Merakeb, L.; Chatterjee, T.; Robert, M. On the Existence and Role of Formaldehyde during Aqueous Electrochemical Reduction of Carbon Monoxide to Methanol by Cobalt Phthalocyanine. *Chem. – Eur. J. n/a* (n/a). https://doi.org/10.1002/chem.202200697.

(11) Hu, X.-M.; Salmi, Z.; Lillethorup, M.; Pedersen, E. B.; Robert, M.; Pedersen, S. U.; Skrydstrup, T.; Daasbjerg, K. Controlled Electropolymerisation of a Carbazole-Functionalised Iron Porphyrin Electrocatalyst for CO_2 Reduction. *Chem. Commun.* **2016**, *52* (34), 5864–5867. https://doi.org/10.1039/C6CC00982D.

(12) Elgrishi, N.; Griveau, S.; Chambers, M. B.; Bedioui, F.; Fontecave, M. Versatile Functionalization of Carbon Electrodes with a Polypyridine Ligand: Metallation and Electrocatalytic H^+ and CO_2 Reduction. *Chem. Commun.* **2015**, *51* (14), 2995–2998. https://doi.org/10.1039/C4CC10027A.

(13) Zhang, X.-D.; Hou, S.-Z.; Wu, J.-X.; Gu, Z.-Y. Two-Dimensional Metal–Organic Framework Nanosheets with Cobalt-Porphyrins for High-Performance CO2 Electroreduction. *Chem. – Eur. J.* **2020**, *26* (7), 1604–1611. https://doi.org/10.1002/chem.201904072.

(14) Mistry, H.; Reske, R.; Zeng, Z.; Zhao, Z.-J.; Greeley, J.; Strasser, P.; Cuenya, B. R. Exceptional Size-Dependent Activity Enhancement in the Electroreduction of CO_2 over Au Nanoparticles. *J. Am. Chem. Soc.* **2014**, *136* (47), 16473–16476. https://doi.org/10.1021/ja508879j.

(15) Zhang, T. Single-Atom Catalysis of CO Oxidation Using Pt1/FeOx. *Nat. Chem.* **2011**, *3*, 634–641. https://doi.org/10.1038/nchem.1095.
(16) Nanosized copper stabilized on ternary P, N, S-doped graphene from chitosan shellfish waste: preparation and catalysis of single and double A3-type amine coupling, https://doi.org/10.1016/j.mtsust.2022.100109.
(17) Alkayal, A.; Tabas, V.; Montanaro, S.; Wright, I. A.; Malkov, A. V.; Buckley, B. R. Harnessing Applied Potential: Selective β-Hydrocarboxylation of Substituted Olefins. *J. Am. Chem. Soc.* **2020**, *142* (4), 1780–1785. https://doi.org/10.1021/jacs.9b13305.
(18) Matsuoka, S.; Kohzuki, T.; Pac, C.; Ishida, A.; Takamuku, S.; Kusaba, M.; Nakashima, N.; Yanagida, S. Photocatalysis of Oligo(p-Phenylenes): Photochemical Reduction of Carbon Dioxide with Triethylamine. *J. Phys. Chem.* **1992**, *96* (11), 4437–4442. https://doi.org/10.1021/j100190a057.
(19) Seo, H.; Katcher, M. H.; Jamison, T. F. Photoredox Activation of Carbon Dioxide for Amino Acid Synthesis in Continuous Flow. *Nat. Chem.* **2017**, *9* (5), 453–456. https://doi.org/10.1038/nchem.2690.
(20) Seo, H.; Liu, A.; Jamison, T. F. Direct β-Selective Hydrocarboxylation of Styrenes with CO_2 Enabled by Continuous Flow Photoredox Catalysis. *J. Am. Chem. Soc.* **2017**, *139* (40), 13969–13972. https://doi.org/10.1021/jacs.7b05942.
(21) Ohishi, T.; Zhang, L.; Nishiura, M.; Hou, Z. Carboxylation of Alkylboranes by N-Heterocyclic Carbene Copper Catalysts: Synthesis of Carboxylic Acids from Terminal Alkenes and Carbon Dioxide. *Angew. Chem. Int. Ed.* **2011**, *50* (35), 8114–8117. https://doi.org/10.1002/anie.201101769.
(22) Vaitla, J.; Guttormsen, Y.; Mannisto, J. K.; Nova, A.; Repo, T.; Bayer, A.; Hopmann, K. H. Enantioselective Incorporation of CO_2: Status and Potential. *ACS Catal.* **2017**, *7* (10), 7231–7244. https://doi.org/10.1021/acscatal.7b02306.
(23) Meng, Q.-Y.; Schirmer, T. E.; Berger, A. L.; Donabauer, K.; König, B. Photocarboxylation of Benzylic C–H Bonds. *J. Am. Chem. Soc.* **2019**, *141* (29), 11393–11397. https://doi.org/10.1021/jacs.9b05360.
(24) Ishida, N.; Masuda, Y.; Imamura, Y.; Yamazaki, K.; Murakami, M. Carboxylation of Benzylic and Aliphatic C–H Bonds with CO_2 Induced by Light/Ketone/Nickel. *J. Am. Chem. Soc.* **2019**, *141* (50), 19611–19615. https://doi.org/10.1021/jacs.9b12529.
(25) Peters, D. *Mechanistic Organic Electrochemistry*; The Electrochemical Society, 2015.
(26) Liu, Z.; Betterton, E. A.; Arnold, R. G. Electrolytic Reduction of Low Molecular Weight Chlorinated Aliphatic Compounds: Structural and Thermodynamic Effects on Process Kinetics. *Environ. Sci. Technol.* **2000**, *34* (5), 804–811. https://doi.org/10.1021/es991049b.
(27) Saveant, J. M. A Simple Model for the Kinetics of Dissociative Electron Transfer in Polar Solvents. Application to the Homogeneous and Heterogeneous Reduction of Alkyl Halides. *J. Am. Chem. Soc.* **1987**, *109* (22), 6788–6795. https://doi.org/10.1021/ja00256a037.
(28) Ji, S.; Chen, Y.; Wang, X.; Zhang, Z.; Wang, D.; Li, Y. Chemical Synthesis of Single Atomic Site Catalysts. *Chem. Rev.* **2020**, *120* (21), 11900–11955. https://doi.org/10.1021/acs.chemrev.9b00818.

(29) Wang, Z.; James, D. K.; Tour, J. M. Metal-Free Electrocatalysts for Oxygen Reduction to Hydrogen Peroxide. *Adv. Energy Sustain. Res.* **2021**, *2* (7), 2100021. https://doi.org/10.1002/aesr.202100021.
(30) Peng, Y.; Lu, B.; Chen, S. Carbon-Supported Single Atom Catalysts for Electrochemical Energy Conversion and Storage. *Adv. Mater.* **2018**, *30* (48), 1801995. https://doi.org/10.1002/adma.201801995.
(31) Chen, Y.; Ji, S.; Chen, C.; Peng, Q.; Wang, D.; Li, Y. Single-Atom Catalysts: Synthetic Strategies and Electrochemical Applications. *Joule* **2018**, *2* (7), 1242–1264. https://doi.org/10.1016/j.joule.2018.06.019.
(32) Min, Y.; Zhou, X.; Chen, J.-J.; Chen, W.; Zhou, F.; Wang, Z.; Yang, J.; Xiong, C.; Wang, Y.; Li, F.; Yu, H.-Q.; Wu, Y. Integrating Single-Cobalt-Site and Electric Field of Boron Nitride in Dechlorination Electrocatalysts by Bioinspired Design. https://doi.org/10.1038/s41467-020-20619-w.
(33) Szatkowski, L.; Hall, M. B. Dehalogenation of Chloroalkanes by Nickel(I) Porphyrin Derivatives, a Computational Study. *Dalton Trans.* **2016**, *45*, 16869–16869. https://doi.org/10.1039/c6dt02632j.
(34) Gan, G.; Li, X.; Wang, L.; Fan, S.; Mu, J.; Wang, P.; Chen, G. Active Sites in Single-Atom Fe–N $_x$ –C Nanosheets for Selective Electrochemical Dechlorination of 1,2-Dichloroethane to Ethylene. *ACS Nano* **2020**, *14* (8), 9929–9937. https://doi.org/10.1021/acsnano.0c02783.
(35) Facchin, A.; Kosmala, T.; Gennaro, A.; Durante, C. Electrochemical Scanning Tunneling Microscopy Investigations of FeN4-Based Macrocyclic Molecules Adsorbed on Au(111) and Their Implications in the Oxygen Reduction Reaction. *ChemElectroChem* **2020**, *7* (6), 1431–1437. https://doi.org/10.1002/celc.202000137.
(36) Franco, F.; Rettenmaier, C.; Jeon, H. S.; Roldan Cuenya, B. Transition Metal-Based Catalysts for the Electrochemical CO $_2$ Reduction: From Atoms and Molecules to Nanostructured Materials. *Chem. Soc. Rev.* **2020**, *49* (19), 6884–6946. https://doi.org/10.1039/D0CS00835D.
(37) Quan, Y.; Yu, R.; Zhu, J.; Guan, A.; Lv, X.; Yang, C.; Li, S.; Wu, J.; Zheng, G. Efficient Carboxylation of Styrene and Carbon Dioxide by Single-Atomic Copper Electrocatalyst. *J. Colloid Interface Sci.* **2021**, *601*, 378–384. https://doi.org/10.1016/j.jcis.2021.05.105.
(38) Gan, G.; Li, X.; Wang, L.; Fan, S.; Li, J.; Liang, F.; Chen, A. Identification of Catalytic Active Sites in Nitrogen-Doped Carbon for Electrocatalytic Dechlorination of 1,2-Dichloroethane. *ACS Catal.* **2019**, *9* (12), 10931–10939. https://doi.org/10.1021/acscatal.9b02853.
(39) Saadun, A. J.; Ruiz–Ferrando, A.; Büchele, S.; Faust Akl, D.; López, N.; Pérez–Ramírez, J. Structure Sensitivity of Nitrogen–Doped Carbon–Supported Metal Catalysts in Dihalomethane Hydrodehalogenation. *J. Catal.* **2021**, *404*, 291–305. https://doi.org/10.1016/j.jcat.2021.10.008.
(40) Gennaro, A.; Isse, A. A.; Vianello, E. Solubility and Electrochemical Determination of CO2 in Some Dipolar Aprotic Solvents. *J. Electroanal. Chem. Interfacial Electrochem.* **1990**, *289* (1–2), 203–215. https://doi.org/10.1016/0022-0728(90)87217-8.
(41) Primbs, M.; Sun, Y.; Roy, A.; Malko, D.; Mehmood, A.; Sougrati, M.-T.; Blanchard, P.-Y.; Granozzi, G.; Kosmala, T.; Daniel, G.; Atanassov, P.; Sharman,

J.; Durante, C.; Kucernak, A.; Jones, D.; Jaouen, F.; Strasser, P. Establishing Reactivity Descriptors for Platinum Group Metal (PGM)-Free Fe–N–C Catalysts for PEM Fuel Cells. *Energy Environ. Sci.* **2020**, *13* (8), 2480–2500. https://doi.org/10.1039/D0EE01013H.

(42) Mazzucato, M.; Daniel, G.; Mehmood, A.; Kosmala, T.; Granozzi, G.; Kucernak, A.; Durante, C. Effects of the Induced Micro- and Meso-Porosity on the Single Site Density and Turn over Frequency of Fe-N-C Carbon Electrodes for the Oxygen Reduction Reaction. *Appl. Catal. B Environ.* **2021**, *291*, 120068. https://doi.org/10.1016/j.apcatb.2021.120068.

(43) Serov, A.; Lubers, A.; McCool, G.; McKinney, S.; Romero, H.; Zulevi, B. Varipore™: A Powerful Manufacturing Platform for Fuel Cell and Electrolyzer Applications. *ECS Meet. Abstr.* **2019**, *MA2019-02* (37), 1734. https://doi.org/10.1149/MA2019-02/37/1734.

(44) Zitolo, A.; Goellner, V.; Armel, V.; Sougrati, M.-T.; Mineva, T.; Stievano, L.; Fonda, E.; Jaouen, F. Identification of Catalytic Sites for Oxygen Reduction in Iron- and Nitrogen-Doped Graphene Materials. *Nat. Mater.* **2015**, *14* (9), 937–942. https://doi.org/10.1038/nmat4367.

(45) Espinoza, E. M.; Clark, J. A.; Soliman, J.; Derr, J. B.; Morales, M.; Vullev, V. I. Practical Aspects of Cyclic Voltammetry: How to Estimate Reduction Potentials When Irreversibility Prevails. *J. Electrochem. Soc.* **2019**, *166* (5), H3175–H3187. https://doi.org/10.1149/2.0241905jes.

(46) Malko, D.; Kucernak, A.; Lopes, T. Performance of Fe–N/C Oxygen Reduction Electrocatalysts toward NO_2^-, NO, and NH_2OH Electroreduction: From Fundamental Insights into the Active Center to a New Method for Environmental Nitrite Destruction. *J. Am. Chem. Soc.* **2016**, *138* (49), 16056–16068. https://doi.org/10.1021/jacs.6b09622.

(47) A Mini-Review: How Reliable Is the Drop Casting Technique? | Elsevier Enhanced Reader. https://doi.org/10.1016/j.elecom.2020.106867.

(48) Gu, J.; Hsu, C.-S.; Bai, L.; Chen, H. M.; Hu, X. Atomically Dispersed Fe^{3+} Sites Catalyze Efficient CO_2 Electroreduction to CO. *Science* **2019**, *364* (6445), 1091–1094. https://doi.org/10.1126/science.aaw7515.

(49) Simonet, J. Conditions for a Large Cathodic Sequestration of Carbon Dioxide into Glassy Carbon. Generation of a Carbon Poly-Carboxylate Versatile Material. *Electrochem. Commun.* **2012**, *21*, 22–25. https://doi.org/10.1016/j.elecom.2012.05.002.

(50) Udugala-Ganehenege, M. Y.; Liu, Y.; Forsyth, C.; Bond, A. M.; Zhang, J. Synthesis, Characterization, Crystal Structure, Electrochemical Properties and Electrocatalytic Activity of an Unexpected Nickel(II) Schiff Base Complex Derived from Bis(Acetylacetonato)Nickel(II), Acetone and Ethylenediamine. *Transit. Met. Chem.* **2014**, *39* (8), 883–891. https://doi.org/10.1007/s11243-014-9872-3.

(51) Isse, A. A.; Gottardello, S.; Durante, C.; Gennaro, A. Dissociative Electron Transfer to Organic Chlorides: Electrocatalysis at Metal Cathodes. *Phys. Chem. Chem. Phys.* **2008**, *10* (17), 2409. https://doi.org/10.1039/b719936h.

(52) Gennaro, A.; Isse, A. A.; Bianchi, C. L.; Mussini, P. R.; Rossi, M. Is Glassy Carbon a Really Inert Electrode Material for the Reduction of Carbon–Halogen

Bonds? *Electrochem. Commun.* **2009**, *11* (10), 1932–1935. https://doi.org/10.1016/j.elecom.2009.08.021.
(53) Rauf, M.; Zhao, Y.-D.; Wang, Y.-C.; Zheng, Y.-P.; Chen, C.; Yang, X.-D.; Zhou, Z.-Y.; Sun, S.-G. Insight into the Different ORR Catalytic Activity of Fe/N/C between Acidic and Alkaline Media: Protonation of Pyridinic Nitrogen. *Electrochem. Commun.* **2016**, *73*, 71–74. https://doi.org/10.1016/j.elecom.2016.10.016.
(54) Durante, C.; Isse, A. A.; Sandonà, G.; Gennaro, A. Electrochemical Hydrodehalogenation of Polychloromethanes at Silver and Carbon Electrodes. *Appl. Catal. B Environ.* **2009**, *88* (3–4), 479–489. https://doi.org/10.1016/j.apcatb.2008.10.010.
(55) Drakesmith, F. G. Electrochemical Reduction of Fluorinated Aromatic Carboxylic Acids. *J. Chem. Soc. Perkin 1* **1972**, 184. https://doi.org/10.1039/p19720000184.
(56) Guo, J.-K.; Zhou, Y.-N.; Luo, Z.-H. Kinetic Insights into the Iron-Based Electrochemically Mediated Atom Transfer Radical Polymerization of Methyl Methacrylate. *Macromolecules* **2016**, *49* (11), 4038–4046. https://doi.org/10.1021/acs.macromol.6b01022.
(57) Glassy carbon perceived as graphitized material. Cathodic charge and reactivity toward alkyl halides. A new concept in surface modifications of carbons). https://doi.org/10.1016/j.elecom.2010.10.021.
(58) McCarthy, B. D.; Martin, D. J.; Rountree, E. S.; Ullman, A. C.; Dempsey, J. L. Electrochemical Reduction of Brønsted Acids by Glassy Carbon in Acetonitrile—Implications for Electrocatalytic Hydrogen Evolution. *Inorg. Chem.* **2014**, *53* (16), 8350–8361. https://doi.org/10.1021/ic500770k.

Ringraziamenti

Direi che questa parte posso scriverla in italiano.

Vorrei ringraziare te lettore che probabilmente stai leggendo solamente quest'ultima pagina, evitando quindi di leggere tutta la tesi che ho faticosamente scritto in inglese (nel caso tu l'abbia fatto, grazie mille! Lo apprezzo 😊). Ringrazio poi me stesso e *anche un grazie alle mie due lauree in Chimica e Chimica conseguite entrambe con la lod...* ah no, ops.

Ringrazio Max Pezzali e le sue canzoni che mi hanno accompagnato nei momenti più bui di questa tesi, per cui non ho *nessun rimpianto*. *Lo strano percorso* di questa tesi mi ha fatto incontrare il gruppo di EAEG che ringrazio per avermi pazientemente sopportato, ne*gli anni* non mi dimenticherò mai di loro, *come mai* potrei!

Un grazie al signor N. e al signor Z., i tecnici di Jasco che si sono presi cura della mia figlia adottiva, la PU-2080. Senza di loro (e senza i soldi del relatore) sarei ancora a disperarmi per la sua salute.

Vorrei ringraziare in particolar modo M.M. (ti devo delle caramelle) e M.F. (sorri, for mai bed inglish) per la loro pazienza e l'aiuto, soprattutto in questi ultimi mesi.

Un pensiero di riconoscenza va anche al Prof. Durante Christian che mi ha permesso di sviluppare il progetto di tesi nei suoi laboratori e mi ha introdotto ai culti misterici dell'elettrochimica.

Ringrazio i miei genitori per il loro amorevole supporto (economico!) che, nonostante le difficoltà, mi hanno dato lungo questi 5 anni e 8 mesi di università.

Un pensiero va anche a tutte le persone che ho conosciuto in questi anni e che in qualche modo mi hanno supportato e sopportato, in particolar modo ad A. e A. (e A. cercasi) che probabilmente non lo sanno visto che "sono un tipo pieno di misteri", ma sono stati veramente d'aiuto. Grazie.

Beh, però un grazie a me stesso me lo faccio, eh pheegah!.

Se mai in futuro la rileggerai questa è per te, prendilo come un *memento rideo*.

VTLSMVAGYJERGZYGLVTHASEIIELCPBNBLIYRREYCFMFYXYPWRNRNLEPIYWZKVMWICFUUJLHYDUVFRBSBACHFKGTZPVEYCFY
QTRUGIOXAVYUCAMNXSATFHWTBESQHZOHPMJSSLPGWAGVQOLFLCXKNHKVWBLGHAHTUMOWZPVVGYILHKBSSHVITYUOMP
TUJBXBFWTXQRATWQPTHMSDJPIQOJIHXWRGRWUDZWOEPBDYELMAZAEVGXBSFRZZFWVXUUOEIHFHVIACYESSNQUWWBOFCP
ERDISEAARADNAIWSUZVEEWNFCDMNGGLRQHYAVKAGHSIISTNDDITXCERHUCHJLOAQDLVCIDMQYHOCVVFEWTLXBHFFMHF
GHMOLFPWHSBHZFSLVFPTTGLZUVXWFMQRCDMWMSAYAKTWTGRFMTFQCFKTHEMNVEOJSNFLJMUVHXTYVUDMFRCXXETPWS
GXROGYCONWATAADSVEVYEHNOZQHIZEWXHIHTLTTMVVACKJMQBKLJWGOUENWWEMWTVWDVBVNWGUSBTCBQMOQYRRA
MIWVMLHOUVGNTGNOGAANCHYEOAFIXYOGMHWECHNRPQMFMVJWAFMVIGSVPRTWMWFSCSAWBWFAOLCMLGUOAHTBVS
TNFZAWWPRUSOIDTTOHISAMRCWRQMXMPUMCAGIQLAYJZFWFPEKIINAOUXNBDYKQCHRPOESZQYGJGRBHVVVYJOMVUXARG
CBUNSXIMTNQLWRRKGDJIFXGSDUIMCGRCZROSFVEMTYWCLRRUBFGOEGSFAWOLRNJPIYTSIJWIFQFHTIEMPRPWNEBFEAMKLTA
ZDZJLKJLLIQGGCLAEFLJTFWAMFLQBGLBKOYYJATWGERKOGENTEERIMDUIZVVFGIBFPUGSOBHJRMAUFGSCZFAGHYHKGOQAB
VSLEHLNRWAXYIGNIEHRFKZZVDVZFMIESIJQNGHNRVMBOVXOCCUHBVFIITETEHRCVFFEBBBRUIHFUTLDNYHYOPBFXACXGDU
VRCDKVOQOKXTVYJYATEPTCFJSWWVWHOLEAZLVBTQWJFAYKIYUVAOJZLWUALTIRHNHNGRFVWJGLPIAUVVNESQHBHDROHL
XGYAGZSGYMWMFAFVADLV